## **PHYSIOLOGY**

# Phosphorylation of RYR1 at Ser<sup>2902</sup> decreases Ca<sup>2+</sup> leak in skeletal muscle and susceptibility to malignant hyperthermia and heat stroke

Rachel Sue Zhen Yee<sup>1</sup>†, Chang Seok Lee<sup>1</sup>†, Ting Chang<sup>1</sup>, Sung Yun Jung<sup>2</sup>, Omar Yousif<sup>1</sup>, Courtney Cavazos<sup>1</sup>, John Colyer<sup>3</sup>, Filip Van Petegem<sup>4</sup>, George G. Rodney<sup>1\*</sup>, Susan L. Hamilton<sup>1\*</sup>

Ryanodine receptor 1 (RYR1) is the sarcoplasmic reticulum (SR) Ca<sup>2+</sup> release channel required for both skeletal muscle contraction and Ca<sup>2+</sup> leak. Mutations in *RYR1* cause malignant hyperthermia susceptibility (MHS) and enhanced sensitivity to heat stroke (ESHS), which can result in death due to excessive skeletal muscle thermogenesis upon exposure to volatile anesthetics or heat. Here, we investigated the molecular and physiological functions of phosphorylation of RYR1 at Ser<sup>2902</sup> by the kinase striated muscle preferentially expressed protein (SPEG). Muscle from SPEG-deficient mice expressing RYR1 with a Ser<sup>2902</sup> Asp<sup>2902</sup> (S2902D) point mutation to mimic phosphorylation by SPEG showed decreased SR Ca<sup>2+</sup> sparks. Muscle from mice homozygous for the S2902D point mutation had reduced SR Ca<sup>2+</sup> transients and small changes in force generation but overall mild phenotypic changes. YS mice, which are heterozygous for a Tyr<sup>524</sup> Ser<sup>524</sup> point mutation in RYR1, show increased Ca<sup>2+</sup> leak and are a model of MHS and ESHS. Crossing YS mice with S2902D mice led to decreased SR Ca<sup>2+</sup> leak and desensitized the mice to both volatile anesthetics and heat. Thus, SPEG inhibits SR Ca<sup>2+</sup> leak in skeletal muscle by phosphorylating Ser<sup>2902</sup> on RYR1, and mutation of Ser<sup>2902</sup> to Asp<sup>2902</sup> to mimic this phosphorylation event rescues YS mice from heat-induced death.

Copyright © 2025 The Authors, some rights reserved; exclusive licensee American Association for the Advancement of Science. No claim to original U.S. Government Works

#### **INTRODUCTION**

The L-type voltage-gated Ca<sup>2+</sup> channel (Ca<sub>V</sub>1.1, also known as the dihydropyridine receptor) interacts with the sarcoplasmic reticulum (SR) Ca<sup>2+</sup> release channel [also known as ryanodine receptor 1 (RYR1)] to, upon transverse tubule depolarization, mechanically open RYR1 to release  $Ca^{2+}$  needed for muscle contraction (1, 2). In addition to its role in excitation-contraction coupling (ECC), RYR1 is the major source of SR Ca<sup>2+</sup> leak (3, 4). Although SR Ca<sup>2+</sup> leak is low in resting muscle, it increases with disease, exercise, and aging and contributes to muscle thermogenesis (5), ECC (6), junctional SR Ca<sup>2+</sup> levels (7, 8), and store-operated Ca<sup>2+</sup> entry (SOCE) (9, 10). Excessive SR Ca<sup>2+</sup> leak is associated with muscular dystrophies (11, 12), malignant hyperthermia susceptibility (MHS) (13, 14), enhanced sensitivity to heat stroke (ESHS) (5, 14-16), metabolic disorders such as hypoglycemia and diabetes (17, 18), and exertional myalgia/rhabdomyolysis (19-23). Elevated SR Ca<sup>2+</sup> leak also contributes to the beneficial effects of exercise (3, 24, 25) and the decline in muscle function with aging (26, 27).

Dominantly inherited mutations in *RYR1* associated with MHS and ESHS cause the channel to display elevated  $Ca^{2+}$  leak and increased sensitivity to activators such as  $Ca^{2+}$ , volatile anesthetics (VAs) (28, 29), heat (14, 30–35), caffeine (36, 37), and statins (38–42). Rycal S48168 (ARM210) (ID NCT04141670), which blocks SR  $Ca^{2+}$  leak, and the antioxidant *N*-acetylcysteine (43, 44) are in clinical trials for RYR1-related diseases (44).

The critical roles of SR Ca<sup>2+</sup> leak in normal and pathological muscle function raise the important questions of what causes and regulates SR Ca<sup>2+</sup> leak in muscle fibers. The Ca<sup>2+</sup> leaky state of RYR1

has been suggested to be the "preopen" state of the channel detected in cryo-electron microscopy (cryo-EM) studies (45), and, therefore, modulators of the channel that stabilize its closed state should decrease Ca<sup>2+</sup> leak. Ca<sub>V</sub>1.1 (46) and the immunophilin FK506 binding protein 12 (FKBP12) (47) stabilize the closed state of RYR1, and a decrease in their interactions with RYR1 increases SR Ca<sup>2+</sup> leak. On the basis of mathematical modeling, it has been hypothesized that Ca<sub>V</sub>1.1 regulates the affinity of a Ca<sup>2+</sup>/Mg<sup>2+</sup> inhibitory site on RYR1, thereby stabilizing the RYR1 closed state in resting muscle (6). Analysis of a mouse model of limb girdle muscular dystrophy shows that the absence of dysferlin decreases the ability of Ca<sub>V</sub>1.1 to control SR Ca<sup>2+</sup> leak and alters the distribution of Ca<sup>2+</sup> among bulk cytosol, SR, and mitochondria (48). Dysferlin deficiency decreases SR Ca<sup>2+</sup> content, Ca<sup>2+</sup> release, and force generation and increases cytosolic Ca<sup>2+</sup> levels, mitochondrial Ca<sup>2+</sup> content, and adenosine 5'-triphosphate synthesis. These studies support roles for  $Ca_V 1.1$  and dysferlin in the regulation of SR  $Ca^{2+}$  leak.

FKBP12 deficiency (49) and major decreases in the interaction of FKBP12 with RYR1 (50) increase RYR1 open probability, indicating that FKBP12 is also a regulator of SR Ca<sup>2+</sup> leak. Because of the high affinity of FKBP12 for RYR1 and the high tissue concentration of FKBP12 (1 to 3  $\mu$ M), a deficiency in FKBP12 in skeletal muscle results in only a 50% decrease in the FKBP12/RYR1 ratio that, nonetheless, increases SR Ca<sup>2+</sup> transients and improves muscle function (51), suggesting that either this alteration does not cause Ca<sup>2+</sup> leak or that a small increase in Ca<sup>2+</sup> leak is actually beneficial to normal muscle function. However, greater decreases in the FKBP12/RYR1 ratio cause SR Ca<sup>2+</sup> leak and have adverse effects on muscle function (47, 49).

SR Ca<sup>2+</sup> leak is also regulated by posttranslational modifications such as oxidation (48, 52, 53) and phosphorylation (50, 54–57). Phosphorylation of RYR1 at Ser<sup>2843</sup> in response to  $\beta$ -adrenergic stimulation has been suggested to decrease the FKBP12/RYR1 interaction and increase SR Ca<sup>2+</sup> leak (50). However, other kinases may also regulate SR Ca<sup>2+</sup> leak. The kinase striated muscle preferentially

<sup>&</sup>lt;sup>1</sup>Department of Integrative Physiology, Baylor College of Medicine, Houston, TX 77030, USA. <sup>2</sup>Department of Biochemistry, Baylor College of Medicine, Houston, TX 77030, USA. <sup>3</sup>Badrilla Ltd., Leeds LS1 3HB, UK. <sup>4</sup>Department of Biochemistry and Molecular Biology, University of British Columbia, Vancouver, BC V6T1Z3, Canada. †These authors contributed equally to this work.

<sup>\*</sup>Corresponding author. Email: susanh@bcm.edu (S.L.H.); rodney@bcm.edu (G.G.R.)

expressed protein (SPEG) interacts with the ECC complex, plays a role in maintaining t-tubule integrity, and stabilizes interactions among ECC proteins in cardiac and skeletal muscle (57-62). SPEG phosphorylates RYR2 to decrease SR Ca<sup>2+</sup> leak (57) and also phosphorylates junctophilin 2 (JPH2) (60, 62) and sarcoplasmic/endoplasmic reticulum Ca<sup>2+</sup> adenosine triphosphatase (SERCA) (61). Therefore, the regulation of leak could also be secondary to changes in SR lumenal Ca<sup>2+</sup> concentration and/or triad stability. We found that SPEG deficiency increases the appearance of Ca<sup>2+</sup> sparks (a consequence of increased Ca<sup>2+</sup> leak) in muscle fibers (58). Ser<sup>2902</sup> on RYR1 has been previously identified to be phosphorylated by SPEG (60). As described in this manuscript, we independently identified Ser<sup>2902</sup> on RYR1 as a SPEG phosphorylation target. On the basis of its identified targets (RYR1, IPH2, and SERCA), SPEG is likely to regulate SR Ca<sup>2+</sup> leak, t-tubule integrity, and reuptake of Ca<sup>2+</sup> into the SR, but the mechanisms of its regulation of SR Ca<sup>2+</sup> leak remain to be fully elucidated.

Mouse models of RYR1 myopathies that display increased SR  $Ca^{2+}$  leak have provided insights into the pathological consequences of SR  $Ca^{2+}$  leak (14, 63–65). A mouse model with a *Ryr1* mutation [*Ryr1*]<sup>Y524S/-</sup> (YS) in mice, *RYR1*]<sup>Y522S/-</sup> in humans] (14) causes MHS and central core disease (66). Muscle fibers in these mice display temperature-dependent increases in cytosolic  $Ca^{2+}$  levels to create a feedforward cycle of increased  $Ca^{2+}$  leak in response to heat or VAs, SERCA activation, mitochondrial  $Ca^{2+}$  uptake, increased heat generation, oxidative stress, and, eventually, massive  $Ca^{2+}$  release, muscle contractures, and death (14, 30). The YS mutation causes the channel to assume a "preactivation" state conformation and to be fully open at a much lower  $Ca^{2+}$  concentration than wild-type (WT) channels by increasing RYR1  $Ca^{2+}$  affinity by ~20-fold (45).

In the current manuscript, we assessed the possibility that SPEG is an endogenous inhibitor of SR  $Ca^{2+}$  leak and generated a mouse model with a mutation at  $Ser^{2902}$  on RYR1 to mimic SPEG phosphorylation of RYR1. The  $Ser^{2902} \rightarrow Asp$  (S2902D) mutation greatly decreased SR  $Ca^{2+}$  leak, and we used it to differentiate between the consequences of SPEG phosphorylation of RYR1 from that of JPH2 and SERCA. We also used these mice to demonstrate the contribution of SR  $Ca^{2+}$  leak to the sensitivity of YS mice to heat and VAs. The S2902D mice are a new tool for assessing the contribution of SR  $Ca^{2+}$  leak to the pathophysiological changes that occur in muscle myopathies.

#### **RESULTS**

# SPEG phosphorylates RYR1 at Ser<sup>2902</sup>

We previously demonstrated using immunoprecipitation and mass spectrometry (MS) that SPEG interacts with RYRs and JPH2 in skeletal muscle triads and cardiac dyads (58). In the current study, we used RYR1 immunoprecipitation assays, MS analysis, and parallel reaction monitoring (PRM) of muscles from SPEG-deficient mice (MCK-Cre<sup>+</sup>Speg<sup>fl/fl</sup>, designated as SPEG-deficient or ΔSPEG) to identify sites of SPEG phosphorylation of RYR1. We consistently found four phosphorylation sites on RYR1 (Ser<sup>2844</sup>, Ser<sup>2902</sup>, Ser<sup>3669</sup>, and Thr<sup>1358</sup>), but only the phosphorylation of Ser<sup>2902</sup> was significantly decreased (57% decrease) in the RYR1 immunoprecipitates from SPEG-deficient mice [Fig. 1, A to D, for phospho-Ser<sup>2844</sup> (p-Ser<sup>2844</sup>), p-Ser<sup>2902</sup>, p-Ser<sup>3669</sup>, and p-Thr<sup>1358</sup>, respectively]. About one-third of total RYR1 was phosphorylated at Ser<sup>2844</sup>, with the other phosphorylation sites representing less than 2% of total RYR1 combined (Fig. 1, A to D). The low phosphorylation of Ser<sup>2902</sup> could indicate that only a subset of channels was targeted by SPEG and/or

that p-Ser<sup>2902</sup> was not stable. Analysis with a polyclonal antibody directed against a p-Ser<sup>2902</sup>–containing RYR1 peptide (fig. S1, A and B) showed that muscle homogenates from SPEG-deficient mice had a 48% reduction in phosphorylation of Ser<sup>2902</sup> in RYR1 compared with those from control mice (Fig. 1E). SPEG deficiency did not completely abolish the phosphorylation of Ser<sup>2902</sup>, suggesting that either residual SPEG [<5% compared with floxed control (FL) mice (58)] in the muscles of these mice maintains some RYR1 phosphorylation or there is a second partially redundant kinase that can phosphorylate RYR1 at this site.

High-resolution cryo-EM has elucidated structural transitions that RYR1 undergoes to assume different functional states (67–70). Thr<sup>2901</sup> (which corresponds to Ser<sup>2902</sup> in mouse) in the cryo-EM structure of rabbit RYR1 (7TZC) is located at the interface between the phosphorylation domain and the bridging solenoid (Bsol), which contains several positively charged residues at the interface (Fig. 1, F and G). Bsol undergoes a major conformational change when RYR1 transitions from the closed to open state (67, 68). This location of Thr<sup>2901</sup> (which is predicted to be less than 4 Å from the positively charged amino acids) suggests that its phosphorylation could affect channel activity, possibly by interacting with these near-by positively charged amino acids.

To assess the functional consequences of phosphorylation of Ser<sup>2902</sup> by SPEG, we created mice with Ser<sup>2902</sup> converted to Asp<sup>2902</sup> (D) to mimic phosphorylation. The heterozygous (*Ryr1*<sup>S2902D/-</sup>) and homozygous (*Ryr1*<sup>S2902D/S2902D)</sup> mice were designated S2902D HET and S2902D HOM, respectively. The p-Ser<sup>2902</sup> antibody also recognized RYR1 in the S2902D HET and S2902D HOM mice (Fig. 1H). We previously reported that muscle fibers from SPEG-deficient (MCK-Cre<sup>+</sup>Speg<sup>fl/fl</sup>) mice display elevated Ca<sup>2+</sup> sparks (58). Isolated flexor digitorium brevis muscles (FDBs) from mice deficient SPEG and also expressing *Ryr1*<sup>S2902D/-</sup> had significantly reduced Ca<sup>2+</sup> spark frequencies (84% decrease) and fewer fibers with Ca<sup>2+</sup> sparks (53% less) compared with FDBs from SPEG-deficient mice (Fig. 1, I to K). Additional phenotyping studies were not performed on these mice because they die by 14 weeks of age from heart failure (59) and RYR1 is not expressed in the heart. The site in RYR2 (Ser<sup>2367</sup>) that is phosphorylated by SPEG in cardiac muscle (57) is not conserved in RYR1, and, likewise, the SPEG phosphorylation site in RYR1 (Ser<sup>2902</sup>) is not conserved in RYR2.

# Phenotyping of the S2902D mice

The finding that the S2902D mutation decreased Ca<sup>2+</sup> sparks in the SPEG-deficient mice raised the question of whether the mutation altered muscle function. We found no differences in body weights at 10 weeks of age (Fig. 2A), but the S2902D HET mice showed a small increase (~19%) in the body fat/body weight ratio with a small decrease (~6%) in the lean weight/body weight ratio compared with S2902D HOM mice (Fig. 2, B and C). We used a comprehensive laboratory animal monitoring system (CLAMS), which showed that WT, S2902D HET, and S2902D HOM mice ate the same amount of food daily (Fig. 2D), but the S2902D HOM mice ran ~42% less on monitored exercise wheels than the S2902D HET mice (Fig. 2, E and F). Moreover, S2902D HOM mice displayed a small ~15% increase in heat generation during the day (Fig. 2G), suggesting the possibility of a metabolic or thermogenic (energy expenditure to maintain body temperature) issue through an unknown mechanism. Using age-matched mice (fig. S2A), we found that body lengths (fig. S2B), bone mineral contents (fig. S2C), and bone mineral densities (fig. S2D)

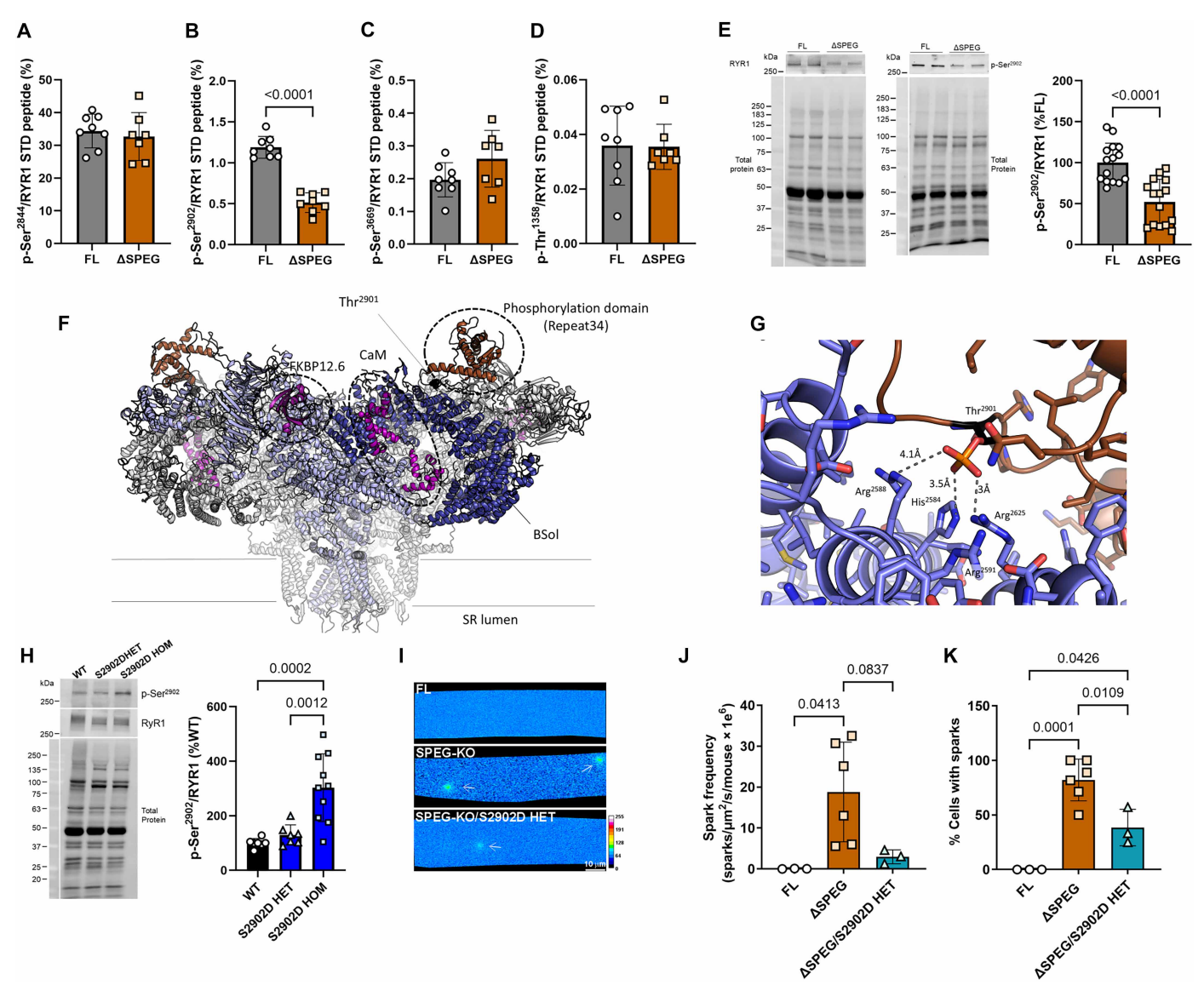
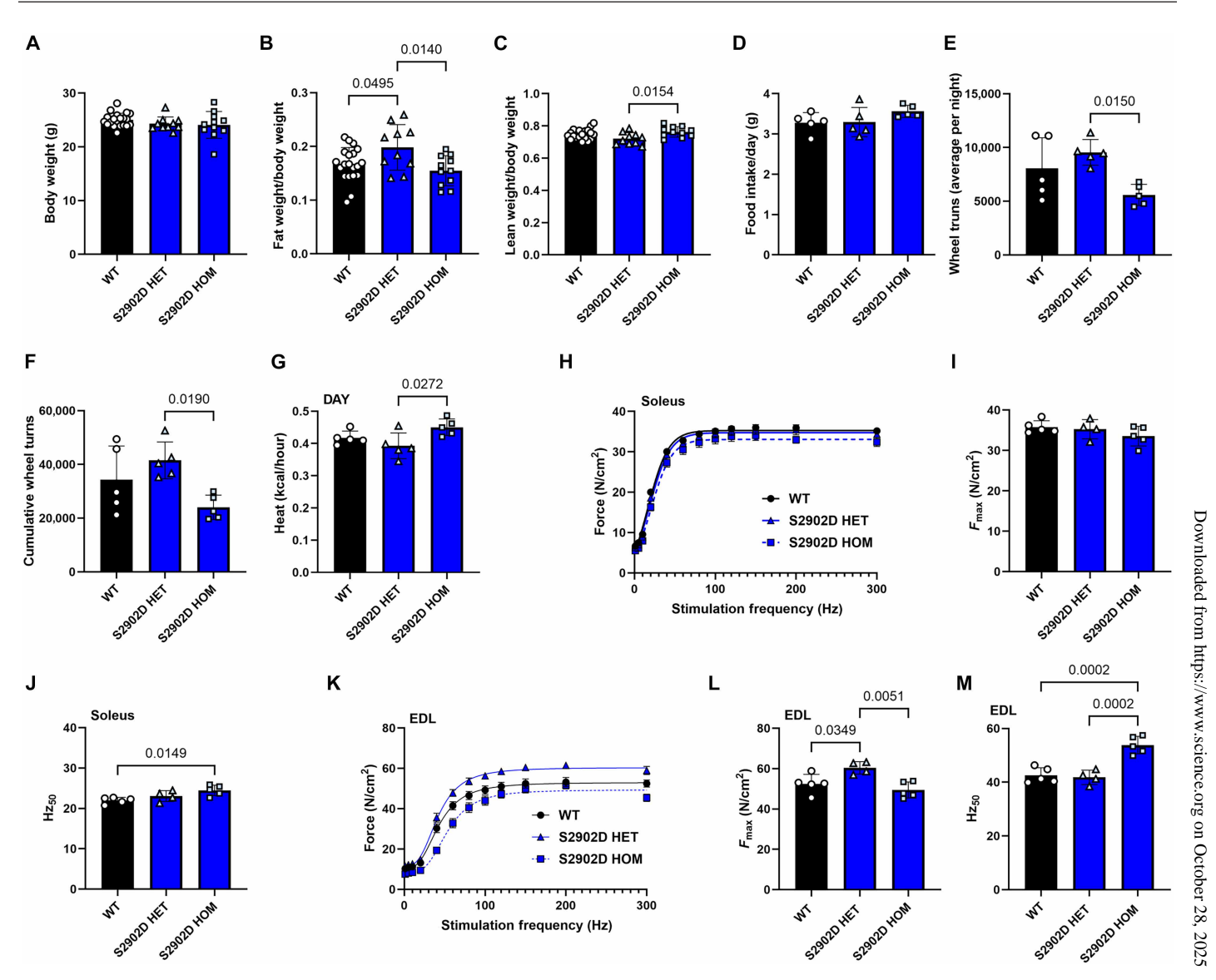


Fig. 1. Phosphorylation of RYR1 on Ser<sup>2902</sup> by SPEG reduces Ca<sup>2+</sup> sparks. (A to D) The phosphorylation sites p-Ser<sup>2844</sup> (A), p-Ser<sup>2902</sup> (B), p-Ser<sup>3669</sup> (C), and p-Thr<sup>1358</sup> (D) on RYR1 identified by RYR1 immunoprecipitation from the gastrocnemius muscles of SPEG-deficient (ΔSPEG) and FL mice (n = 8 animals per group), MS, and PRM using the procedures that we have previously described (*58*). Percentage of phosphorylation was estimated by dividing intensity-based absolute quantification (iBAQ) values for the phosphorylated peptide from PRM by the amount of RYR1 in that immunoprecipitate, which was defined as the average of the three most highly recovered RYR1 peptides in each immunoprecipitate, × 100. (E) Immunoblotting for p-Ser<sup>2902</sup> in homogenates from TA muscles from ΔSPEG and FL mice. Data were normalized to RYR1 and corrected for batch effects by plotting as % FL (mean) for that specific experiment (n = 15 animals per group). (F) Three-dimensional structure of rabbit RYR1 (Protein Data Bank: 7TZC) with Thr<sup>2901</sup> (which corresponds to Ser<sup>2902</sup> in mouse) located at the interface between the bridging solenoid domain (BSOI) and phosphorylation domain (right dotted circle). (G) Thr<sup>2901</sup> (in black) in rabbit RYR1 points toward the BSOI region, close to several positively charged residues (labeled). Estimated distance is indicated. Side chains are shown as sticks, and nitrogen and oxygen atoms are colored as dark blue and red, respectively. (H) Immunoblotting for p-Ser<sup>2902</sup> in TA muscle homogenates from WT (n = 5), S2902D HET (n = 7), and S2902D HOM (n = 10) mice. (I) Ca<sup>2+</sup> sparks in FDB fibers of FL (n = 3), ΔSPEG (n = 6), and ΔSPEG/S2902D HET (n = 3) mice. (J) Ca<sup>2+</sup> spark frequency. (K) Percentage of fibers with Ca<sup>2+</sup> sparks. All mice used for this figure were 8- to 10-week-old male mice. Data are plotted as means  $\pm$  SD, and n = 10 values were determined by unpaired n = 10 to one-way ANOVA [(H), (J), and (K)].

of S2902D mice were unchanged compared to control mice. CLAMS parameters, including average ambulation at night (fig. S3A) or during the day (fig. S3B), average heat at night (fig. S3C) or during the day (fig. S3D), average  $VO_2$  (volume of oxygen consumed) at night (fig. S3E) or during the day (fig. S3F), average  $VCO_2$  (volume of carbon dioxide produced) at night (fig. S3G) or during the day (fig. S3H), and average respiratory exchange ratio at night (fig. S3I) or during the day

(fig. S3J), displayed either no differences or only small changes among the three genotypes.

We evaluated the effects of the HET and HOM S2902D mutation on the ability of the muscles in 10- to 12-week-old mice to generate force. S2902D HET and S2902D HOM soleus muscles did not differ in maximal force generation (Fig. 2, H and I), but the half maximal stimulation frequency (Hz $_{50}$ ) of S2902D HOM soleus



**Fig. 2. Phenotyping of the male S2902D mice.** (**A** to **C**) Body compositions of WT (n = 20), S2902D HET (n = 10), and S2902D HOM (n = 11) male mice at 10 weeks of age. Body weight (A). Fat weight/body weight (B). Lean weight/body weight (C). (**D** to **G**) Metabolic and activity data for WT (n = 5), S2902D HET (n = 5), and S2902D HOM (n = 5) mice from CLAMS. Average food intake (D). Activity shown as average wheel turns at night determined with monitored exercise wheel (E). Cumulative wheel turns (F). Average heat during the day (G). (**H** to **M**) Ex vivo muscle function of male mice. Force (newtons per square centimeter) generated as a function of stimulation frequency for the soleus muscle (H). Maximal force ( $F_{max}$ ) generation in the soleus muscle (I). Hz<sub>50</sub> (J). Force generated as a function of stimulation frequency for EDL muscle (K). Maximal force generation in EDL muscle (L). Hz<sub>50</sub> (M). For (H) and (I), n = 5 WT, n = 4 S2902D HET, and n = 5 S2902D HOM mice. For (K) to (M), n = 5 WT, n = 4 S2902D, and n = 5 S2902D HOM mice. Force frequency curves [(H) and (K)] were fit with four-parameter sigmoidal functions (lines). Data in bar graphs (obtained from the curve fits) are plotted as means  $\pm$  SD. Data in force-frequency curves are plotted as means  $\pm$  SEM for visualization purposes. P values are indicated as analyzed by one-way ANOVA with Tukey's multiple comparisons test.

muscles displayed a small rightward shift of  $\sim$ 3 Hz compared with that of WT soleus muscles (Fig. 2, H and J). The extensor digitorum longus (EDL) muscles from S2902D HET mice displayed an  $\sim$ 15% increase in maximal force generation compared with WT EDL muscles. Maximal force for S2902D HOM EDL muscles was less (18%) than that of S2902D HET EDL muscles (Fig. 2, K and L) but not significantly different from that of WT EDL muscles. The EDL muscle force frequency curve for S2902D HOM mice displayed a significant  $\sim$ 11- to 12-Hz rightward shift in the Hz<sub>50</sub> compared with those for WT and S2902D HET mice (Fig. 2, K and M). S2902D HET or HOM

female mice (at 10 to 12 weeks of age) did not differ from WT mice in body weights (fig. S4A) and showed similar changes in muscle function to those of S2902D HET or HOM male mice when compared to female WT mice (fig. S4, B to G).

# The S2902D mutation in RYR1 decreases SR Ca<sup>2+</sup> release and leak

We evaluated the effects of the S2902D mutation in RYR1 of electrically evoked Ca<sup>2+</sup> transients using Mag-Fluo-4 as the fluorescent Ca<sup>2+</sup> indicator in FDB fibers at 25°C (Fig. 3, A and B). Both HET and

HOM S2902D mutation reduced the amplitude of Ca<sup>2+</sup> transients by 22 and 27%, respectively (Fig. 3C), without altering the half-maximal stimulation frequency (Fig. 3D), which is consistent with a stabilization of the closed state of the channel.

To further define the functional consequences of the S2902D mutation, we crossed the S2902D mice with the YS model of MHS/

ESHS, which displays elevated SR Ca<sup>2+</sup> leak (*14*, *15*, *30*, *71*), to generate YS/S2902D mice (heterozygous for both YS and S2902D). Measurement of the resting cytosolic Ca<sup>2+</sup> concentrations in Fura-2-loaded FDB fibers showed a small (6%) but significant increase in resting Ca<sup>2+</sup> in fibers from YS mice compared with fibers from WT, S2902D HET, and YS/S2902D mice (Fig. 3E). When the temperature

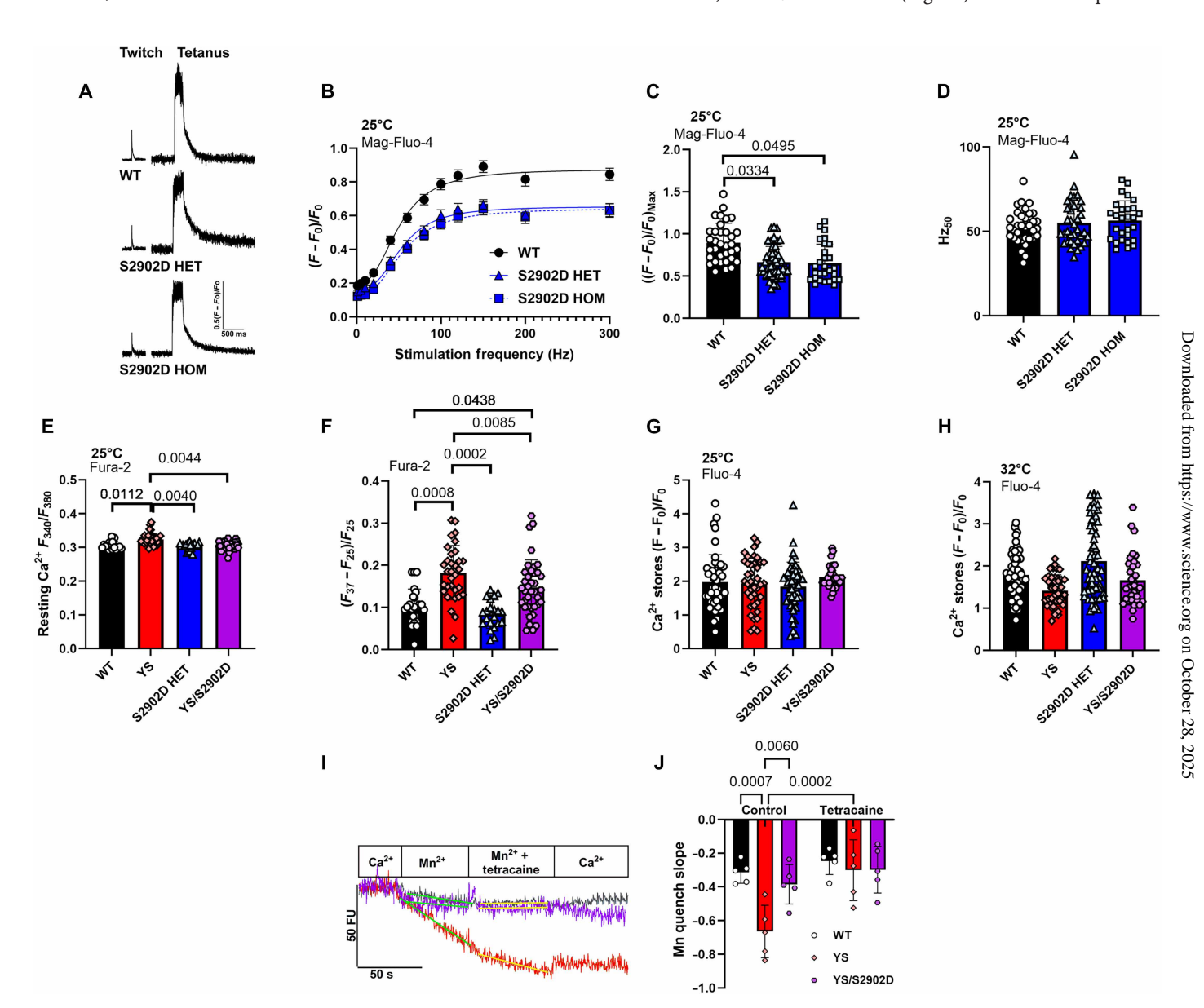


Fig. 3. The effect of the S2902D mutation in RYR1 on  $Ca^{2+}$  handling. (A to D) FDB fibers isolated from mice were loaded with the  $Ca^{2+}$  fluorescent indicator Mag-Fluo-4 to measure voltage-activated whole-cell  $Ca^{2+}$  transients (25°C). (A) Representative traces of 1- and 150-Hz stimulation from each genotype. (B)  $Ca^{2+}$ -frequency curve, (C) peak  $Ca^{2+}$ , and (D)  $Hz_{50}$  for WT (34 fibers from n=4 mice), S2902D HET (34 fibers from n=5 mice), and S2902D HOM (28 fibers from n=5 mice). Both peak  $Ca^{2+}$  and  $Hz_{50}$  were determined by four-parameter sigmoidal curve fits [line in graph, (B)]. (E) Resting cytosolic  $Ca^{2+}$  determined using Fura-2 for WT (17 fibers from n=5 mice), YS (34 fibers from n=6 mice), S2902D HET (21 fibers from n=5 mice), and YS/S2902D (39 fibers from n=6 mice) mice. (F) The change in fluorescence (resting  $Ca^{2+}$ ) when temperature was elevated to 37°C compared with 25°C. (G) Assessment of relative  $Ca^{2+}$  stores at 25°C using Mag-Fluo-4. WT (46 fibers from n=4 mice), YS (39 fibers from n=4 mice), S2902D HET (46 fibers from n=4 mice), and YS/S2902D (29 fibers from n=3 mice) mice. (H) Assessment of relative  $Ca^{2+}$  stores at 32°C using Mag-Fluo-4. WT (50 fibers from n=4 mice), YS (40 fibers from n=4 mice), S2902D HET (58 fibers from n=4 mice), and YS/S2902D (36 fibers from n=4 mice). WT (50 fibers from n=4 mice), S2902D HET (58 fibers from n=4 mice), and YS/S2902D (36 fibers from n=4 mice). WT (50 fibers from n=4 mice), S2902D HET (58 fibers from n=4 mice), and YS/S2902D (36 fibers from n=4 mice). WT (50 fibers from n=4 mice), S2902D HET (58 fibers from n=4 mice), and YS/S2902D (36 fibers from n=4 mice). YS (red, n=5 mice) mice. (I) Representative Mn<sup>2+</sup> quench of cytoplasmic Fura-2 fluorescence at 360 nm in the absence and presence of tetracaine (1 mM) for WT (black, n=5 mice), YS (red, n=5 mice), and YS/S2902D (purple, 39 fibers from n=5 mice) mice. (J) Summary of the rate of Mn<sup>2+</sup> quench in the absence and

of the perfusate was raised to 37°C, YS fibers showed an ~2-fold increase in the resting cytosolic Ca<sup>2+</sup> concentration compared with WT and S2902D mice (Fig. 3F), thus demonstrating the temperature dependence of the SR Ca<sup>2+</sup> leak in YS mice. The resting Ca<sup>2+</sup> in YS fibers was only ~1.2-fold higher than that in YS/S2902D fibers, consistent with the S2902D mutation being heterozygous and some of the RYR1 tetramers having the YS but not the S2902D mutation. The resting cytosolic Ca<sup>2+</sup> concentration in S2902D HET fibers did not significantly differ from that in WT fibers. We also used ICE solution (72) to release Ca<sup>2+</sup> from SR stores in Mag-Fluo-4–loaded FDB fibers. We did not detect a difference in SR Ca<sup>2+</sup> stores at 25°C (Fig. 3G) or at 32°C (Fig. 3H) in YS fibers compared to that in WT fibers.

We also used tetracaine to block SR  $Ca^{2+}$  leak from RYR1 in passive  $Mn^{2+}$  quench studies performed with FDB (Fig. 3I). The  $Mn^{2+}$  quench rate was greatest in FDB fibers from YS mice, which was decreased by both tetracaine and the S2902D mutation (Fig. 3J). The faster tetracaine-sensitive  $Mn^{2+}$  quench rate in YS FDB fibers suggests that elevated SR  $Ca^{2+}$  leak either increases the number of constitutively active store-operated channels (73) or causes local store depletion-activated  $Ca^{2+}$  influx (74).

# ECC proteins are decreased in abundance in YS muscle but restored by the S2902D mutation

The YS mutation in RYR1 caused increased SR Ca2+ leak but decreased levels of ECC proteins. RYR1 levels were reduced by 31% in YS muscle but were restored to WT levels in YS/S2902D muscle (Fig. 4A). The S2902D mutation by itself did not alter RYR1 levels (Fig. 4A). p-Ser<sup>2902</sup>/RYR1 levels did not significantly differ in YS and WT muscles but increased by 26% in YS/S2902D muscle compared with those in S2902D HET muscle. Although the p-Ser<sup>2902</sup> antibody is likely to have a different affinity for p-Ser<sup>2902</sup> RYR1 than for S2902D RYR1, an increase in the immunolabeling in muscles of YS/ S2902D mice compared with S2902D HET mice (which presumably have the same S2902D RYR1 content) may indicate an increase in p-Ser<sup>2902</sup> in the muscles of YS/S2902D mice (Fig. 4B). RYR1 was not the only ECC protein decreased in YS muscle but not in YS/S2902D muscle. Other proteins showing similar changes included  $Ca_V 1.1\alpha 1s$ (Fig. 4C), SPEGβ (Fig. 4D), SPEGα (Fig. 4E), JPH1 (Fig. 4F), and JPH2 (Fig. 4G). Because JPH2 is cleaved by calpain (58, 75-77), we used antibodies that recognized either the N or C terminus of JPH2. The antibody that recognized the C terminus of JPH2 detected a 92-kDa fragment (Fig. 4, G and H) that was increased in YS muscle and restored to WT levels in YS/S2902D muscle, suggesting that the decrease in JPH2 is likely due to calpain-mediated cleavage.

# The YS and/or S2902D mutations in RYR1 alter calmodulin and FKBP12 interactions with RYR1

We identified RYR1-binding proteins by MS analysis of RYR1 immunoprecipitates from gastrocnemius muscle (Fig. 5, A to E). Specific RYR1-binding proteins identified in the immunoprecipitates (in approximate order of abundance) included FKBP12, calmodulin (CaM), alpha-2-macroglobulin like 1 protein [a serine protease inhibitor (78) also known as BC048546], SPEG, obscurin, and JPH2. Because of the large variations in protein recoveries among immunoprecipitations, we pooled data (such that each protein was normalized to the amount of RYR1 in that specific immunoprecipitation) from eight independent immunoprecipitations (Fig. 5, F to K). Despite the variability, these studies provided insight into the amount of each protein recovered in the immunoprecipitates without

correcting for batch effects. There were only two significant differences. The first was that the amount of FKBP12 was lower in RYR1 immunoprecipitates from YS muscle (the mice that display the greatest Ca<sup>2+</sup> leak among the mice in this study) than in those from S2902D HOM muscle (the mice that display the least SR Ca<sup>2+</sup> leak among the mice in this study), supporting the role of FKBP12 in suppressing Ca<sup>2+</sup> leak. The second was that the amount of CaM was lower in RYR immunoprecipitates from YS mice than in those from YS/S2902D mice, suggesting that the S2902D mutation can restore CaM binding to RYR1 with the YS mutation.

# YS and YS/S2902D muscles show comparable and unimpaired force generation, but YS/S2902D muscle shows decreased caffeine sensitivity compared with YS muscle

Neither maximal force nor  $Hz_{50}$  differed for either soleus (Fig. 6, A to C) or EDL muscles (Fig. 6, D to F) in YS and YS/S2902D mice. For comparison, we replotted the maximal force and  $Hz_{50}$  values for WT, S2902D HET, and S2902D HOM mice (Fig. 2, I and L) together with those for YS and YS/S2902D mice (Fig. 6, B and E, and fig. S5, A to D). We did not detect genotype-specific differences in maximal force or  $Hz_{50}$  in soleus muscles. Maximal force of the EDL muscles did not differ among WT, S2902D HET, S2902D HOM, YS, and YS/S2902D mice, but the  $Hz_{50}$  values for S2902D HOM EDL muscles were significantly different from those for the EDL muscles of YS and YS/S2902D mice (fig. S5D). The  $Hz_{50}$  values for YS or S2902D EDL muscles did not differ from those of WT EDL muscles.

An in vitro contracture test (IVCT), which is commonly used to diagnose MHS/ESHS, assesses the caffeine sensitivity of biopsied muscle (79-82). To determine whether the S2902D mutation altered the response of muscle to caffeine, we attached isolated soleus and EDL muscles to force transducers and measured passive tension in response to increasing concentrations of caffeine. Both YS soleus (Fig. 6, G and H) and EDL (Fig. 6, I and J) muscles responded at much lower caffeine concentrations than those from WT mice (>50 mM for WT compared with ~10 to 22 mM for YS). The IVCT value for YS/ S2902D soleus muscle displayed a small but significant shift to higher caffeine concentrations compared with that for YS soleus muscle. The S2902D mutation in the absence of the YS mutation also decreased the response to caffeine. The IVCT value for EDL muscle displayed a larger shift to the right in the YS/S2902D mice compared with that in the YS mice (Fig. 6, I and J). However, the caffeine response of YS/ S2902D mice differed from that of WT mice, suggesting that the S2902D HET mutation may decrease Ca<sup>2+</sup> sensitivity of RYR1 in the presence of the YS mutation but does not restore it to WT affinity.

# The S2902D mutation decreases the sensitivity of YS mice to heat and VAs

YS mice undergo a life-threatening hypermetabolic response to both heat and VAs. We sought to determine whether decreasing SR  $\rm Ca^{2+}$  leak with the S2902D mutation rescued YS mice from exposure to heat and/or VAs. We measured VO<sub>2</sub> as a function of time in unanesthetized mice exposed to 37°C for 15 min. Changes in VO<sub>2</sub> were used to measure the hypermetabolic response of awake mice to avoid death as an end point, and we measured rectal temperature immediately after the heat challenge. YS mice displayed an 80% increase in VO<sub>2</sub> (Fig. 7, A and B) and 3°C higher body temperature (Fig. 7C) than WT mice, responses not seen in the YS/S2902D mice (Fig. 7, A to C).

To assess the MH response to VAs, we exposed mice on a warming pad set at 36°C to the VA isoflurane for 30 min. If a warming pad

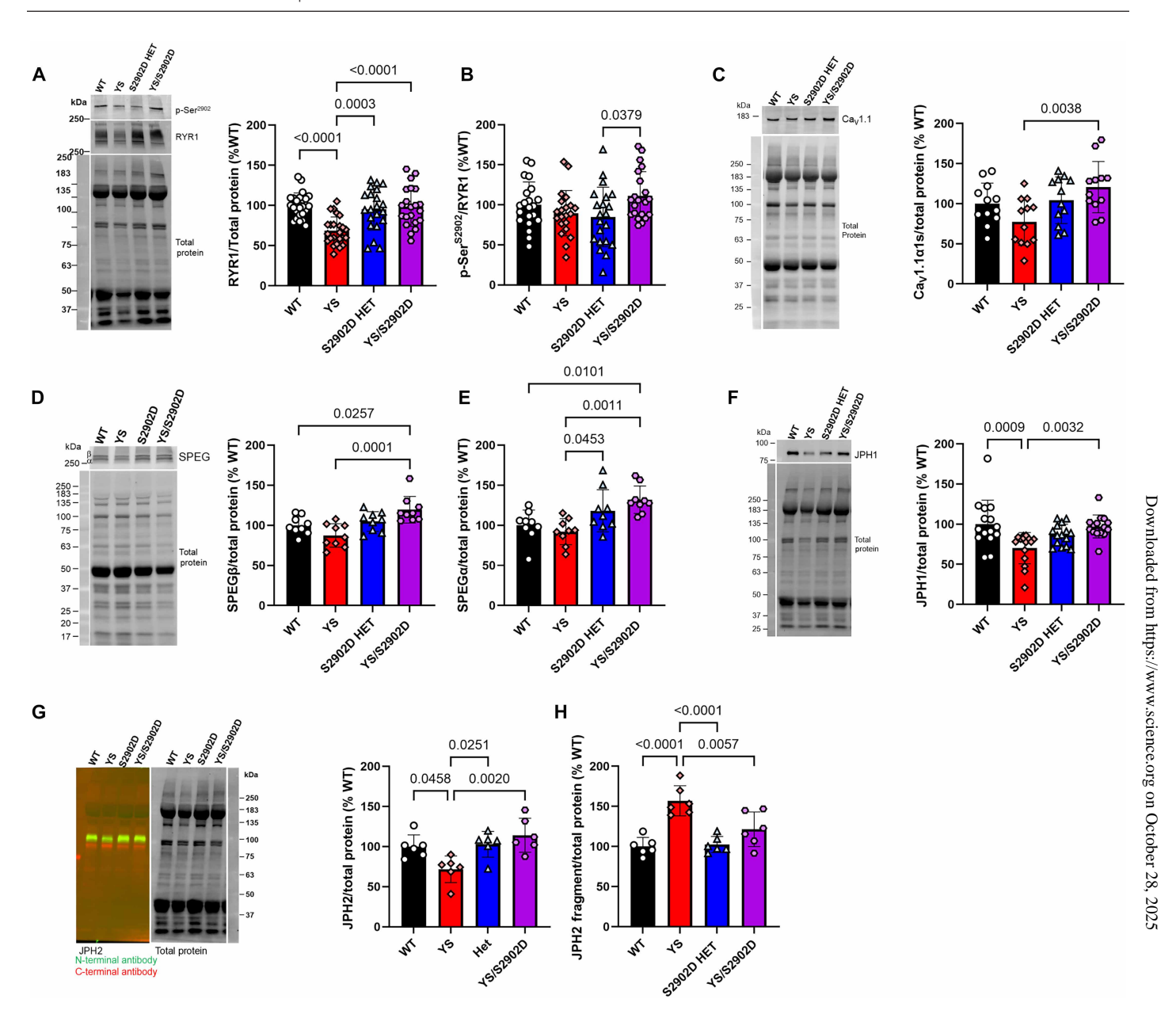


**Fig. 4. Changes in the abundance of ECC proteins by the YS and S2902D mutations.** (**A**) Representative Western blot for RYR1 and p-Ser<sup>2902</sup> in RYR1. Graph shows quantification of RYR1/total protein, presented as % WT (n = 24 WT, n = 24 YS, n = 21 S2902D HET, and n = 21 YS/S2902D mice). (**B**) Graph shows quantification of p-Ser<sup>2902</sup>/RYR1, presented as % WT (n = 21 mice per genotype). (**C**) Representative Western blot and summary plot for Ca<sub>V</sub>1.1α1s. Graph shows quantification of Ca<sub>V</sub>1.1α1s/total protein, presented as % WT (n = 12 mice per genotype). (**D**) Representative Western blot for SPEGβ (top band) and SPEGα (lower band). Graph shows quantification of SPEGβ/total protein, presented as % WT (n = 9 mice per genotype). (**E**) Graph shows quantification of SPEGα/total protein, presented as % WT (n = 9 mice per genotype). (**E**) Graph shows quantification of SPEGα/total protein, presented as % WT (n = 9 mice per genotype). (**G**) Representative Western blot using antibodies to the N terminus (green) and the C terminus (red) of JPH2. The upper band (red) is full-length JPH2 and the lower band (green) is a ~92-kDa fragment [JPH2 runs more slowly than predicted on SDS gels (58)]. Graph shows quantification of JPH2 (full length)/total protein, presented as % of WT. (**H**) Graph shows quantification of the C-terminal fragment of JPH2/total protein, presented as % of WT. For (G) and (H), n = 6 mice per genotype. All mice used for this figure were 8- to 12-week-old male mice. Data are plotted as means  $\pm$  SD. P values were determined by one-way ANOVA with Tukey's multiple comparisons test.

is not used and body temperature is allowed to drop during VA exposure, then YS mice do not respond to VAs (14). We measured rectal temperature (Fig. 7, D and E) and muscle temperature in the gastrocnemius muscle during isoflurane exposure (Fig. 7, F and G). YS mice displayed a large increase in both body (~6°C increase) (Fig. 7E) and muscle temperatures (~6°C increase) (Fig. 7G)

at the end of the heat challenge. However, YS/S2902D mice displayed a delayed response to isoflurane (<2°C increase in body temperature at 15 min), and none died during the isoflurane exposure. The YS/S2902D mice had a higher overall survival rate than YS mice (all of which died around 15 min of isoflurane exposure) (Fig. 7H). Although none of the YS/S2902D mice died

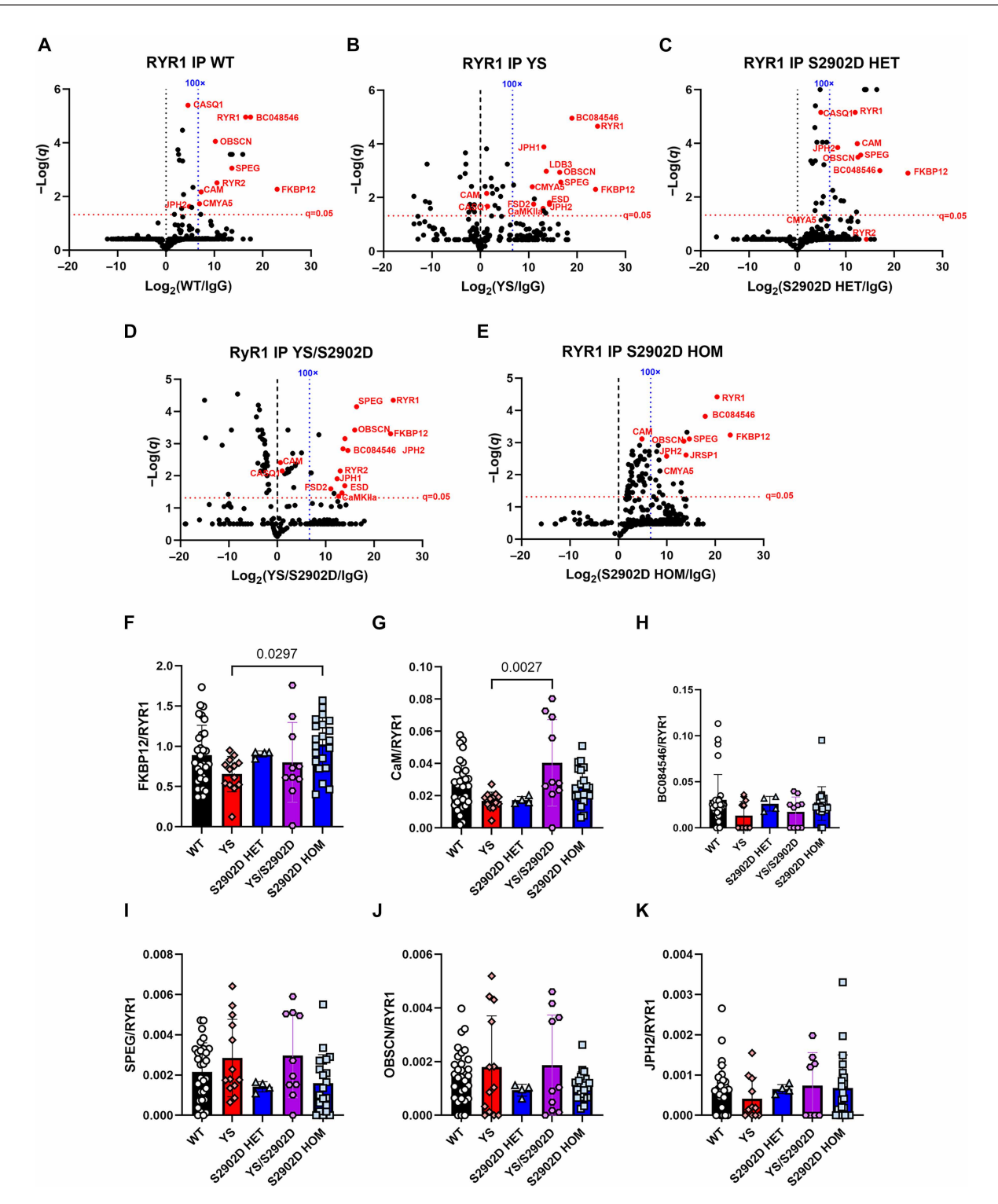
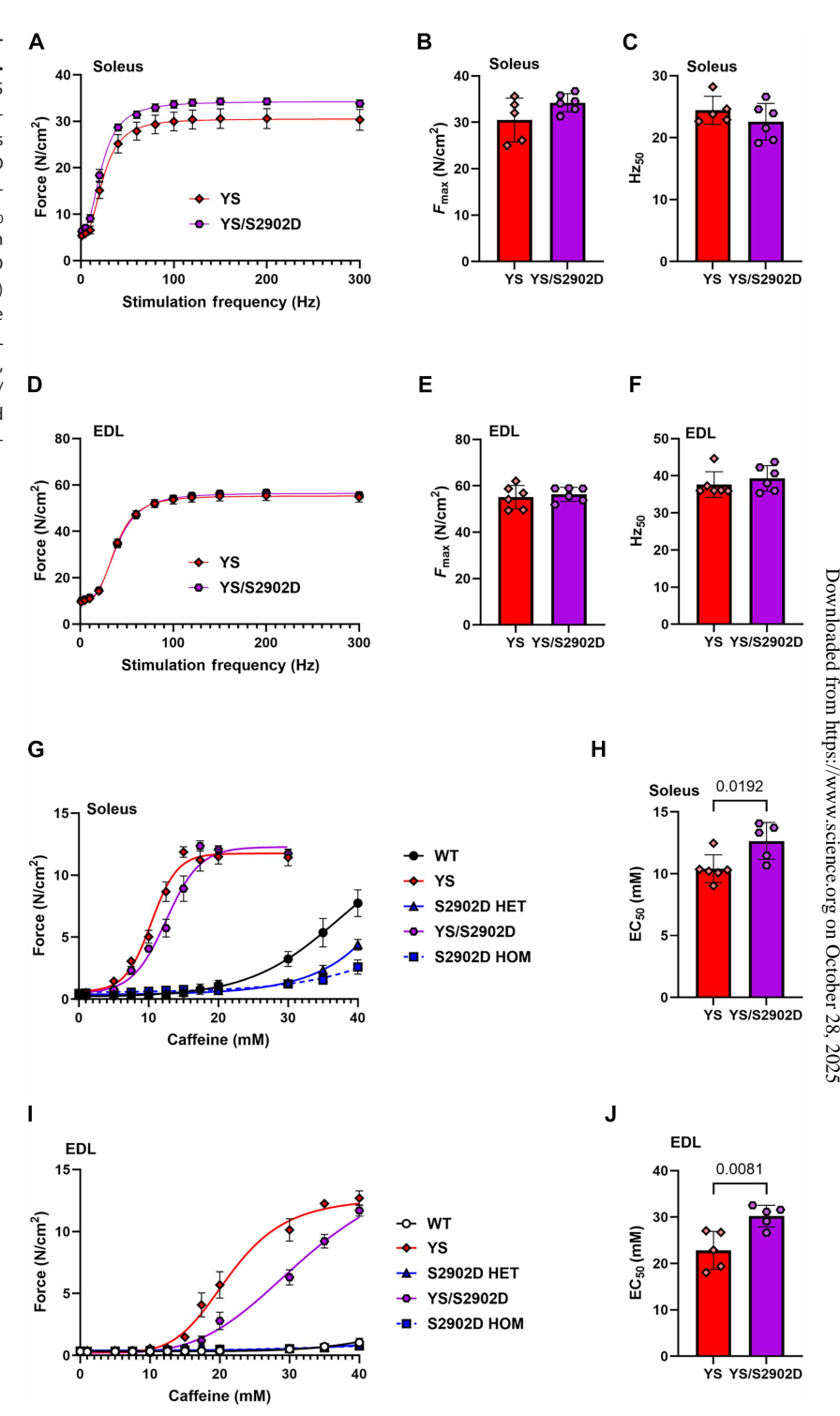


**Fig. 5. Effects of the S2902D mutation on RYR1-binding proteins.** RYR1 was immunoprecipitated from NP-40 solubilized homogenates of gastrocnemius muscles of WT, YS, S2902D HET, YS/S2902D, and S2902D HOM mice. Proteins in the immunoprecipitates (IPs) were identified by MS, and ECC proteins are labeled in red. q is the FDR. Data in each panel were compared with IgG nonspecific controls obtained for that specific IP. (**A**) Volcano plot of RYR1-binding proteins in WT muscle  $(n_{\text{animals}} = 8)$ . (**B**) Volcano plot of RYR1-binding proteins in YS muscle  $(n_{\text{animals}} = 4)$ . (**C**) Volcano plot of RYR1-binding proteins in S2902D HET muscle  $(n_{\text{animals}} = 8)$ . (**D**) Volcano plot of RYR1-binding proteins in YS/S2902D muscle  $(n_{\text{animals}} = 4)$ . (**E**) Volcano plot of RYR1-binding proteins in S2902D HOM muscle  $(n_{\text{animals}} = 8)$ . (**F**) Volcano plot of RYR1-binding proteins in S2902D HOM muscle  $(n_{\text{animals}} = 8)$ . (**F**) Volcano plot of RYR1-binding proteins in S2902D HOM muscle  $(n_{\text{animals}} = 8)$ . (**F**) Volcano plot of RYR1-binding proteins in S2902D HOM muscle  $(n_{\text{animals}} = 8)$ . (**F**) Volcano plot of RYR1-binding proteins in S2902D HOM muscle  $(n_{\text{animals}} = 8)$ . (**F**) Volcano plot of RYR1-binding proteins in S2902D HOM muscle  $(n_{\text{animals}} = 8)$ . (**F**) Volcano plot of RYR1-binding proteins in S2902D HOM muscle  $(n_{\text{animals}} = 8)$ . (**F**) Volcano plot of RYR1-binding proteins in S2902D HOM muscle  $(n_{\text{animals}} = 8)$ . (**F**) Volcano plot of RYR1-binding proteins in S2902D HOM muscle  $(n_{\text{animals}} = 8)$ . (**F**) Volcano plot of RYR1-binding proteins in S2902D HOM muscle  $(n_{\text{animals}} = 8)$ . (**F**) Volcano plot of RYR1-binding proteins in S2902D HOM muscle  $(n_{\text{animals}} = 8)$ . (**F**) Volcano plot of RYR1-binding proteins in S2902D HOM muscle  $(n_{\text{animals}} = 8)$ . (**F**) Volcano plot of RYR1-binding proteins in S2902D HOM muscle  $(n_{\text{animals}} = 8)$ . (**F**) Volcano plot of RYR1-binding proteins in S2902D HOM muscle  $(n_{\text{animals}} = 8)$ . (**F**) Volcano plot of RYR1-binding pro

Fig. 6. Comparison of force generation and caffeine sensitivity of the soleus and EDL muscles of YS and YS/S2902D mice. (A) Force frequency curves for YS and YS/S2902D muscles (n = 5mice per genotype). (B) Maximal force generation in soleus muscles of YS and YS/S2902D mice from (A). (C) Hz<sub>50</sub> values for soleus muscles from (A). (D) Force frequency curves for YS and YS/S2902D EDL muscles (n = 6 mice per genotype). (E) Maximal force generation in EDL muscles of YS and YS/S2902D mice from (D). (F) Hz<sub>50</sub> values for EDL muscles from (D). (G) Force generated as a function of caffeine concentration in WT, YS, S2902D HET, and YS/S2902D soleus muscles. (H) Caffeine mean effective concentration (EC50) values for YS and YS/S2902D soleus muscles from (G). (I) Caffeine curves for WT, YS, S2902D HET, YS/S2902D, and S2902D HOM EDL muscles. For (G) and (H), n = 4 WT, 5 YS, 3 S2902D HET, 5 YS/S2902D, and 3 S2902D HOM mice. (J) EC<sub>50</sub> values for caffeine for YS and YS/ S2902D EDL muscles. Bar graphs are plotted as means  $\pm$  SD, and curves are plotted as means ± SEM. P values determined by unpaired t tests. All mice were between 10 and 12 weeks of age.



during the VA exposure, some mice died immediately after the iso-flurane exposure.

#### **DISCUSSION**

SPEG, a member of the myosin light change kinase family, is a kinase with two kinase domains that is preferentially expressed in

cardiac and skeletal muscle (83), and SPEG deficiency is a cause of centronuclear myopathy and dilated cardiomyopathy (84, 85). SPEG-deficient mice die of heart failure before 14 weeks of age but also show severely impaired skeletal muscle function (62, 85). In skeletal muscle, SPEG deficiency disrupts triads and decreases both Ca<sub>V</sub>1.1-dependent Ca<sup>2+</sup> influx and RYR1-dependent Ca<sup>2+</sup> transients (59). SPEG also has multiple targets, raising the question of

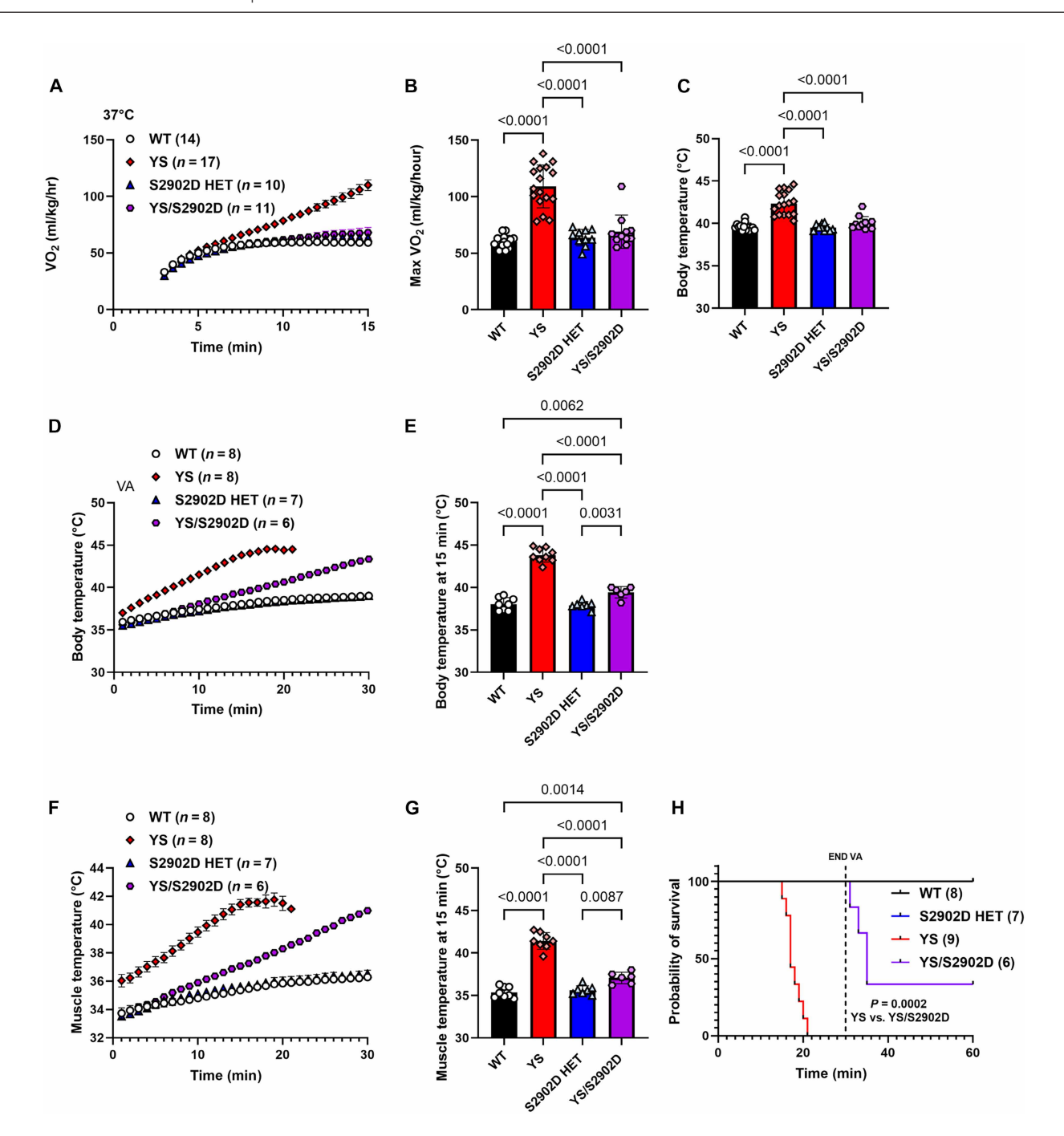


Fig. 7. Effect of the S2902D mutation on the sensitivity of YS mice to heat and VAs. (A)  $VO_2$  during heat challenge (37°C for 15 min). n = 14 WT, 17 YS, 10 S2902D HET, and 11 YS/S2902D mice. (B and C) Maximal  $VO_2$  (B) and body temperature (C) taken with a rectal thermometer of the mice after the heat challenge. (D to H) Mice were exposed to VAs for 30 min, and rectal and gastrocnemius muscle temperatures were recorded each minute. n = 8 WT, 8 YS, 7 S2902D HET, and 6 YS/S2902D mice. Body temperatures during the VA challenge measured with rectal thermometer (D). Body temperatures at the 15-min time point (E). Temperatures of the gastrocnemius muscles during VA exposure (F) and at the 15-min time point (G). Survival rates of mice exposed to VA (H). Mice were 8- to 12-week-old male mice. Bar graphs are plotted as means  $\pm$  SD, and curves are plotted as means  $\pm$  SEM. P values determined by one-way ANOVA with Tukey's multiple comparisons test [(B), (C), (E), and (G)] or Mantel-Cox log-rank test (H).

which targets cause the functional changes in muscles in SPEG-deficient mice. In cardiac and skeletal muscles, SPEG phosphorylates RYRs (57, 59, 60, 62), JPH2 (57, 62), and SERCA (61), and SPEG phosphorylation of RYR2 decreases SR Ca<sup>2+</sup> leak (57). SPEG deficiency alters the phosphorylation of both JPH2 at multiple sites and RYR1 at Ser<sup>2902</sup> (60). We found that SPEG deficiency in skeletal

muscle fibers increases Ca<sup>2+</sup> sparks (58) and decreased phosphorylation of Ser<sup>2902</sup> on RYR1. To elucidate the role of SPEG in muscle, not only do its targets need to be identified but also the mechanisms that regulate SPEG activation need to be elucidated. SPEG has a CaM binding motif (83), and if Ca<sup>2+</sup> binding to CaM activates SPEG, then this could represent a feedforward cycle to limit Ca<sup>2+</sup>

leak. However, SPEG appears to be able to phosphorylate at least one of its targets (JPH2) in vitro in the absence of  $Ca^{2+}$  (62).

A complication in defining SPEG targets using SPEG-deficient mice is the possibility of redundant kinases. A greater than 90% decrease in SPEG produces only a 50 to 60% decrease in Ser<sup>2902</sup> phosphorylation [(60) and the current study], suggesting that there is likely to be a second kinase that can phosphorylate RYR1 at Ser<sup>2902</sup>. One such potential candidate for this redundant kinase is obscurin (OBSCN), which, like SPEG, is a dual kinase of the myosin lightchain kinase family. Our studies support this possibility because obscurin is specifically immunoprecipitated with RYR1 (58), but additional studies are needed to assess this possibility.

We created mice with a S2902D mutation in RYR1 to mimic phosphorylation. S2902D HOM mice displayed substantially reduced voluntary running on monitored exercise wheels. Moreso than soleus muscles, EDL muscles in these mice showed a greater impairment in the ability to generate force and a rightward shift in the force-frequency curve. Muscle fibers from both S2902D HET and S2902D HOM mice had decreased  $\text{Ca}^{2+}$  transients but no changes in the Hz<sub>50</sub>. These findings are consistent with the S2902D mutation stabilizing the closed state of RYR1. The rightward shift in the muscle force frequency curves is likely due to inadequate  $\text{Ca}^{2+}$  being released at the lower frequencies to trigger adequate contraction.

SR Ca<sup>2+</sup> leak is low in resting control muscle fibers, but even small increases have functional consequences (3). To determine whether phosphorylation of Ser<sup>2902</sup> by SPEG truly reduced SR Ca<sup>2+</sup> leak, we crossed the S2902D mice with YS (*Y524S*<sup>+/-</sup>) mice, a model of MHS and ESHS with enhanced SR Ca<sup>2+</sup> leak (*14*, *30*, *71*). We detected a small (6%) increase in resting cytosolic Ca<sup>2+</sup> in YS fibers compared with WT, S2902D HET, and YS/S2902D fibers. This difference in resting Ca<sup>2+</sup> was increased almost twofold at 37°C. In contrast, the YS/S2902D mice did not display an increase in resting Ca<sup>2+</sup> at room temperature and had a smaller increase in resting Ca<sup>2+</sup> than YS mice at 37°C, supporting a role of phosphorylation of RYR1 by SPEG in reducing SR Ca<sup>2+</sup> leak in skeletal muscle and suggesting that some channels in YS/S2902D mice still display heat-induced SR Ca<sup>2+</sup> leak, possibly because of some YS leaky channels not having the S2902D mutation because the S2902D mutation is heterozygous in these mice.

To further assess Ca<sup>2+</sup> leak, we used Mn<sup>2+</sup> quench of Fura-2 fluorescence in FDBs at 25°C. We found an increased rate of Mn<sup>2+</sup> quench in YS muscle that was blocked by both tetracaine (which blocks RYR1-mediated Ca<sup>2+</sup> leak) and the S2902D mutation, suggestive of increases in both SR Ca<sup>2+</sup> leak and Ca<sup>2+</sup> entry. SR Ca<sup>2-</sup> leak and local Ca2+ store depletion can activate low levels of SOCE in skeletal muscle (74, 86). The increased Ca<sup>2+</sup> entry in YS fibers could be due to this mechanism (74), increased constitutively active SOCE (73), and/or increased Ca<sup>2+</sup> entry through Ca<sub>V</sub>1.1. Additional studies are needed to distinguish between these mechanisms. We (71) and others (87) have shown that the increased SR  $Ca^{2+}$  leak leads to decreased SR Ca<sup>2+</sup> stores. Despite this reduction in SR Ca<sup>2+</sup>, we did not observe a reduction in voltage-activated force at 25°C, consistent with previous reports (14). This preservation of force is likely due to a redistribution of intracellular Ca<sup>2+</sup>, given that we did not detect differences in ICE-inducible Ca<sup>2+</sup> stores at either 25° or 32°C. These data are consistent with those obtained from a mouse model of MHS with the G2435R mutation (74).

The pronounced functional effects of the S2902D mutation on  $\mathrm{Ca}^{2+}$  leak raise the question of how this mutation affects the structure

of RYR1. From the position of Thr<sup>2901</sup> in RYR1 from cryo-EM studies, phosphorylated Thr<sup>2901</sup> might interact with nearby (<4 Å) positively charged amino acids to form a salt bridge with Arg<sup>2588</sup>, His<sup>2584</sup>, and/or Arg<sup>2625</sup> to stabilize a closed, nonleaky state of the channel. The YS mutation in RYR1 increases its Ca<sup>2+</sup> affinity of RYR1 by ~20-fold (45), whereas the S2902D mutation decreases caffeine sensitivity of YS muscle but also reduces the response to caffeine in muscle without the YS mutation. Because caffeine binding to RYR1 is Ca<sup>2+</sup>-dependent (88), these data indirectly support decreased Ca<sup>2+</sup> affinity of RYR1 in the muscles of YS/S2902D mice as part of the mechanism by which the S2902D mutation (and Ser<sup>2902</sup> phosphorylation) stabilizes the closed state of the channel and reduces SR Ca<sup>2+</sup> leak.

The abundance of RYR1 (31% decrease) and other ECC proteins (10 to 30% decreases) is reduced in YS muscle but is restored by the S2902D mutation. The decreased ECC protein levels could be due to Ca<sup>2+</sup> activation of calpains because Ca<sup>2+</sup>-activated proteases target ECC proteins when cytosolic Ca<sup>2+</sup> levels increase (89–92). Consistent with a role for calpain-mediated cleavage of ECC proteins, we showed a decrease in full-length JPH2 and a 50% increase in a JPH2 fragment in YS muscle that was restored to WT levels in YS/S2902D muscle.

Stabilization of the closed state of the channel could be due to changes in the interactions of RYR1 with modulators, and proteins that stabilize the closed state of the channel would be predicted to have lower affinities for preopen and open channels compared with the closed channel. If this is true, then RYR1 with the YS mutation should bind to less FKBP12 and Ca<sub>V</sub>1.1. Because only small amounts of Ca<sub>V</sub>1.1α1s coimmunoprecipitated with RYR1, we were unable to determine whether the YS or S2902D mutations altered Ca<sub>V</sub>1.1 interactions with RYR1. However, the FKBP12/RYR1 level was lowest in YS muscle (the mice with the greatest RYR1 Ca<sup>2+</sup> leak) and greatest in S2902D HOM muscle (likely to be the mice with the least SR Ca<sup>2+</sup> leak), supporting the stabilization of the closed channel by FKBP12 (47). The only other notable change was in the CaM/RYR1 ratio that was higher in YS/S2902D muscle than in YS muscle. Compared with the FKBP12 results, this finding is more difficult to interpret because CaM is a partial agonist at low Ca<sup>2+</sup> and a channel inhibitor at high Ca<sup>2+</sup> (93–98) but seems to remain bound to RYR1 through Ca<sup>2+</sup> concentration changes.

In vitro studies with gene editing of Ser<sup>2844</sup> to block its phosphorylation by protein kinase A (PKA) demonstrate that blocking a phosphorylation event that increases RYR1 activity can be used to decrease SR Ca<sup>2+</sup> leak associated with MHS mutations in RYR1 (99). In the current study, we mutated  $Ser^{2902}$  to  $Asp^{2902}$  to mimic a phosphorylation event in mice with a leaky RYR1 mutation (Tyr<sup>+/524S</sup>), which showed that blocking SR Ca<sup>2+</sup> leak desensitized YS mice to heat and VAs. This combination of mutations decreased Ca<sup>2+</sup> leak in FDB fibers, decreased caffeine sensitivity of EDL and soleus muscles, and restored ECC protein levels compared with YS mice. However, this combination of mutation did not alter the ability of isolated soleus or EDL muscles to generate force. The S2902D mutation decreased the response of the YS mice to both VAs and heat, thereby increasing survival rates. Because the S2902D mutation was heterozygous in YS/S2902D mice, phenotype rescue was not complete because heat increased Ca<sup>2+</sup> leak in muscle fibers from these mice, but the overall leak was lower than in YS muscle fibers.

Increased SR Ca<sup>2+</sup> leak has been detected not only in other dominantly inherited RYR-related diseases but also in other muscle

diseases such as muscular dystrophy (11, 74, 100). S2902D mice could be used to directly test the role of SR Ca<sup>2+</sup> leak in mouse models of these myopathies. Another important future use of S2902D mice will be to define the contributions of SR Ca<sup>2+</sup> leak to the beneficial effects of exercise, the decline in muscle function with aging, thermogenesis, and metabolism. Our studies suggest that the development of drugs that activate SPEG could have potential to treat muscle diseases with increased Ca<sup>2+</sup> leak.

#### **MATERIALS AND METHODS**

#### **Experimental design**

The objective of the study was to evaluate the role of Ca<sup>2+</sup> leak in normal and diseased skeletal muscle function. We performed in vivo experiments to test the response of the mice to heat and VAs, ex vivo muscle function in response to electrical stimulation and caffeine, and single muscle fibers to assess changes in Ca<sup>2+</sup> transients and sparks and used frozen muscle samples for biochemistry experiments. Individuals performing functional test were blinded to mouse identities/ treatments and the order of mice tested was randomized.

#### Mice

All animal experiments in this study were approved by the Institutional Animal Care and Use Committee (IACUC) at Baylor College of Medicine under IACUC protocol AN-2656 and AN-5829. Newly created or recently received mice were extensively backcrossed and maintained on C57BL/6J genetic background. The creation of the Ryr1<sup>Y524S/+</sup> (YS) mice (MGI:3619253) was previously described (14). Floxed SPEG (Speg<sup>fl/fl</sup>, FL) mice were obtained from ES cell clone EPD0180\_2\_A07 from the Knockout Mouse Phenotyping Program (KOMP) repository (RRID:MMRRC062855-UCD) (101) and generated by the Wellcome Trust Sanger Institute. B6.FVB(129S4)-Tg (Ckmm-cre) 5Khn/J (MCK-Cre<sup>+</sup>) mice (102) were purchased from the Jackson Laboratory (RRID:IMSR\_JAX:006475, Bar Harbor, Maine). MCK Cre<sup>+</sup> mice were maintained in a hemizygous state before mating with floxed SPEG mice. All in vivo data were obtained with at least three independent experimental animal cohorts, and mice were randomized and the experimenter was blinded with respect to mouse identity before experiments were performed and during data analyses. Mouse littermates were used in most experiments, and, where not possible, age-matched controls were used. For rigor and reproducibility, n was calculated using 80% power ( $\alpha$ , 0.05) and from previous or preliminary studies. The number of mice used in each experiment is indicated in each figure legend.

# CRISPR-mediated knock-in allele design and reagent production for S2902D mice

To define the functional consequences of SPEG-mediated phosphorylation of Ser<sup>2902</sup>, we created using CRISPR-Cas9 editing a mouse model in which Ser<sup>2902</sup> was mutated to an aspartic acid (S2902D) to mimic phosphorylation. S2902D mice were generated in collaboration with BCM (Baylor College of Medicine) GERM Core (fig. S6). A single guide RNA (gRNA) was selected using the Wellcome Trust Sanger Institute Genome Editing website to target a double-strand break proximal to Ser<sup>2902</sup> [chr7:29068152-29068174 (GRCm38), CRISPR ID 513005517]. The gRNA was synthesized by Synthego (Redwood City, CA). The gRNA chosen had no predicted off-target sites with less than three-base mismatches in exons or on the same

chromosome. To introduce the Asp<sup>2902</sup> mutation and a nonsynonymous mutation for the novel Bcl I site, a donor DNA template was synthesized by Integrated DNA Technologies (IDT, Coralville, IA) as an ultramer. Single gRNA and Cas9 protein (PNA Bio) were precomplexed before adding the repair donor into a mix for electroporation into C57BL/6J mouse zygotes as described previously (103). We validated the S2902D mutation in these mice using Sanger sequencing. After multiple backcrosses on the C57BL/6J background, we analyzed the functional consequences of the S2902D mutation.

#### Genotyping of S2902D mice

Allele characterization was performed by polymerase chain reaction (PCR) to identify founders with the targeted S2902D mutation, whose genomic DNA was subjected to Sanger sequencing. PCR reaction was performed using primers (forward, 5′- GGGGCGAAAGAAGAAGCAAG; and reverse, 5′- CCACTTGCAGGTCCTTAGGT) and restriction digest of the PCR product with Bcl I. Mice were backcrossed for at least three generations before being used for experiments.

#### **Metabolic measurements**

CLAMS experiments were performed as previously described (15).

#### **Heat response**

Heat challenge experiments were performed as previously described (15). Room humidity and temperature were monitored in all experiments.

#### VA exposure

Mice were exposed to 2% isoflurane mixed with  $O_2$  for 30 min at a constant flow of 2 lpm and placed on a  $36^{\circ}\text{C}$  heated pad. This non-triggering temperature was used to maintain the body temperature of the mice. Body temperature was assessed with RightTemp rectal thermometer (PhysioSuite, Kent Scientific). A sterile thermocouple fabricated into a 29-gauge needle (MT-29/2HT, World Precision Instruments) was inserted  $\sim 0.5$  cm into the gastrocnemius muscle to monitor muscle temperature. Signs of stress and survival of mice were continuously monitored up to 48 hours after isoflurane exposure.

#### **Body composition**

Mice were anesthetized with 100 mg of ketamine/10 mg of xylazine per kilogram of body weight and assessed using the dual-energy x-ray absorptiometry system (DEXA, Faxitron).

## Ex vivo force measurements and caffeine response

Mice were anesthetized with 100 mg of ketamine/10 mg of xylazine per kilogram of body weight and euthanized by cervical dislocation. Soleus and EDL muscles were dissected from the mice. Using a 4-0 silk suture, one tendon of each muscle was securely tied to a fixed hook and the other tendon was fastened to a force transducer (F30; Harvard Apparatus). Muscles were placed in a physiological saline solution containing 120.0 mM NaCl, 4.0 mM KCl, 1.8 mM CaCl<sub>2</sub>, 1.0 mM MgSO<sub>4</sub>, 25.0 mM NaHCO<sub>3</sub>, 1.0 mM KH<sub>2</sub>PO<sub>4</sub>, and 10.0 mM glucose (pH 7.3), and continuously gassed with 95% O<sub>2</sub>–5% CO<sub>2</sub> at 25°C. Muscles were incubated at 25°C for 10 min, and optimal length ( $L_0$ ) was obtained. For force measurements, voltage ( $V_{\rm max}$ ) was adjusted to elicit maximal twitch force. Muscles were stimulated at frequencies of 1, 5, 10, 20, 40, 60, 80, 100, 120, 150, 200, and 300 Hz (0.5-ms pulse duration and 250-ms train duration) at 1-min intervals. For caffeine response, muscles were exposed to caffeine

concentrations of 0, 1, 5, 7.5, 10, 12.5, 15, 17.4, 20, 30, 35, 40, 45, and 50 mM for 3 min per concentration, and force was measured as the mean over the last 30 s of each concentration. Muscle weight and  $L_0$  were used to estimate cross-sectional area, and absolute forces were expressed in newtons per square centimeter (104).

#### **Dissociation of FDB**

Intact FDBs were dissected from mice and incubated in Dulbecco's modified Eagle's medium (DMEM; 10569-010, Thermo Fisher Scientific) and collagenase (3 to 4 mg/ml; C0130, Sigma-Aldrich) at 37°C for 1 hour. Isolated fibers were transferred to DMEM supplemented with 10% FBS, antibiotic/antimycotic (100×) (15240062, Thermo Fisher Scientific) and 25 mM Hepes and incubated in 5%  $\rm CO_2$  at 25°C overnight.

# Ca<sup>2+</sup> transients

For voltage-activated whole-cell  $\text{Ca}^{2+}$  transients, isolated FDB myofibers were loaded with the low-affinity  $\text{Ca}^{2+}$  dye Mag-Fluo-4-AM (10 µm; Invitrogen), for 30 min at 25°C in Hepes-Ringer containing 120.0 mM NaCl, 4.7 mM KCl, 1.8 mM  $\text{CaCl}_2$ , 0.6 mM MgSO<sub>4</sub>, 1.6 mM NaHCO<sub>3</sub>, 0.13 mM NaH<sub>2</sub>PO<sub>4</sub>, 10.0 mM glucose, and 20.0 mM Hepes. The fibers were washed three times in dye-free Hepes-Ringer and the dye was deesterified for 20 min at 25°C. FDB myofibers were stimulated at 1, 5, 10, 20, 40, 60, 80, 100, 120, 150, and 300 Hz (0.5-ms pulse duration and 250-ms train duration) and Mag-Fluo-4 fluorescence [excitation (Ex), 488/30 nm; and emission (Em), 535/40 nm] was monitored using IonOptix Myocyte Calcium and Contractility Recording System (IonOptix, Westwood) at 1000 Hz.

## Ca<sup>2+</sup> influx and SR Ca<sup>2+</sup> leak

For resting cytosolic Ca<sup>2+</sup> measurements isolated FDB myofibers were loaded with Fura-2-AM (5 μm; Invitrogen) for 30 min at 25°C in Hepes-Ringer. The myofibers were washed three times in dye-free Hepes-Ringer, and the dye was deesterified for 20 min at 25°C. Fibers were placed in a temperature controlled perfusion system (PH-6D, Warner Instruments) equipped with an in-line solution heater (SH-27B, Warner Instruments), and temperature was controlled with the dual channel temperature controller (TC-344C, Warner Instruments). Fura-2 fluorescence (Ex, 340/12 and 380/12 nm; and Em, 510/40 nm) was monitored using a Myocyte Calcium and Contractility Recording System (IonOptix, Westwood) at 250 Hz. Fibers were held for 2 min at 25°C that was ramped to 37°C over 5 min and were maintained at 37°C for 2 min. The fluorescence within 2 min at 25° and 37°C was averaged to obtain the 340/380 ratio as a function of temperature. For Mn<sup>2+</sup> quench studies, FDBs were perfused with Hepes-Ringer followed by replacing the CaCl<sub>2</sub> solution with a Mn<sup>2+</sup>-Hepes solution (1.8 mM MnCl<sub>2</sub>), and the quench of Fura-2 fluorescence (Ex, 360/12 nm; and Em, 510/40 nm) was assessed in the absence and presence of the RyR blocker, tetracaine (1 mM, Sigma-Aldrich). The rate of Fura-2 quench at 360 nm was calculated by subtracting the basal slope in the presence of Ca<sup>2+</sup> from the slope during application of Mn<sup>2+</sup> (±tetracaine) and expressed as fluorescence units (FU) per second. Mn<sup>2+</sup> quenches Fura-2 fluorescence at all wavelengths, but the quench at 360 nm is independent of cytosolic Ca<sup>2+</sup> levels and, therefore, measures the influx of divalent cations across the sarcolemma.

# Ca<sup>2+</sup> stores

Isolated FDB myofibers were loaded with Mag-Fluo-4-AM (5  $\mu m;$  Invitrogen) for 20 min at either 25° or 32°C in Hepes-Ringer solution.

The fibers were washed three times in dye-free Hepes-Ringer, and the dye was deesterified for 20 min at either 25° or 32°C. Baseline recordings were obtained for 2 min. Fibers were perfused with a Ca<sup>2+</sup>-free Hepes-Ringer solution containing 10 μM ionomycin (Tocris), 30 μM cyclopiazonic acid (CPA, Tocris), and 100 µM EGTA (ICE cocktail) (72, 105), and images were recorded for 5 min. All solutions were supplemented with 40 μM N-benzyl-p-toluenesulfonamide (BTS, Tocris) to inhibit muscle contraction and were maintained at 25° or 32°C. The temperature of the chamber and platform was maintained using a temperature-controller and heated platform (TC-344B, PH-6D, SH-27B, CC-28, Warner Instruments). FDB fibers were imaged with an inverted Nikon Eclipse TE-200 microscope equipped with a Lambda DG5 illumination system and a Photometrics camera. Mag-Fluo-4 was excited at 488 nm (10-ms exposure), and emitted light was collected at >510 nm with a frame rate of 50 ms. Images were recorded using µManager software (UCSF) and analyzed using the ImageJ plugin (National Institutes of Health). Cells with less than a 50-FU response above the fluorescence in the absence of ICE the cocktail were eliminated from data analysis.

## Ca<sup>2+</sup> sparks in living fibers

Experiments were performed as previously described with minor modifications (58). Isolated FDB myofibers were loaded with Fluo-4-AM (5  $\mu$ m) in Hepes-Ringer solution for 20 min at 25°C, washed three times with dye-free Hepes-Ringer solution, and rested for 20 min at 25°C for dye deesterification. High-resolution images were obtained on a Zeiss-LSM 780 with a 40× numerical aperture 1.2 water objective. Pixel dimensions were 0.21  $\mu$ m by 0.21  $\mu$ m in the x and y dimensions. A sequence of 60 XY images was collected over time (963.4 ms per frame), and sparks frequency was determined as previously described (58).

#### **Immunoprecipitation assays**

Immunoprecipitation assays were performed as previously described (58, 61). Gastrocnemius muscles from S2902D HET, S2902D HOM, YS, YS/S2902D, and WT mice were homogenized in 10 volumes of immunoprecipitation buffer (w/v) [50 mM tris-HCl (pH 7.4), 170 mM NaCl, 1 mM EDTA, and 1% NP-40] containing protease and phosphatase inhibitors using a bead homogenizer (Precellys tissue homogenizer). Using a total  $Ca^{2+}$  of 2.7 mmol/kg of wet weight in fast twitch mouse skeletal muscle (106) and MaxChelator (107), we estimated the free  $Ca^{2+}$  in the MS/immunoprecipitate to be <10 nM.

## MS and PRM

MS and PRM were performed as previously described with minor modifications (58, 108). MS data were acquired using a combined method of data-dependent acquisition (DDA) and PRM within the same MS run. A list of the PRM target peptides is provided in table S1. Full MS scans were acquired in the Orbitrap across a mass range of 300 to 1400 mass/charge ratio at a resolution of 120,000. Higher-energy collisional dissociation was used to generate MS/MS spectra in the ion trap using rapid scan mode for DDA. PRM scans were concurrently performed for selected target peptides to facilitate precise quantification. Data analysis was conducted as previously described with minor modifications (58, 108). The precursor mass tolerance was set to 20 parts per million, and the fragment mass tolerance was 0.5 Da. Up to two missed cleavages were allowed, along with dynamic modifications for N-terminal acetylation and methionine oxidation.

# Creation and testing of the antibody to p-Ser<sup>2902</sup> in RYR1

To create an antibody specific to RYR1 phosphorylated at Ser<sup>2902</sup>, the structure of this region in mouse, rabbit (Protein Data Bank: 7KOS; although the residue is Thr instead of Ser), and human RYR1 was compared. The phosphorylation site is solvent accessible, and an epitope sequence of 2887AKGGGSHPL2905 (murine residue numbering) was a first candidate for the immunogen (fig. S1, A and B). Additional sequence at the C terminus is hydrophobic and likely to be buried. Additional sequence at the N terminus is highly charged and well structured. However, the structure is unlikely to form in a short peptide, and the charged nature of any extension could dominate immunogenicity, thus demoting the importance of the phosphorylated serine residue. The sequence AKGGGSHPL was BLAST searched against a murine database, which returned only RYR1, RYR3, and RYR2 in mouse. RYR2 does not have a phosphorylatable residue at the position equivalent to Ser<sup>2902</sup>.

An immunogen peptide of Ac-2887AKGGGS\*HPL2905Camide (where S\* denotes phospho-serine) was synthesized using 9-luorenyl methoxycarbonyl (Fmoc) chemistry and purified to 98.56% purity [as assessed by peak area integration of high-performance liquid chromatography (HPLC) spectrogram and supported by liquid chromatography (LC)-MS spectra]. The immunogen peptide was conjugated to the C-terminal cysteine residue to keyhole limpet hemocyanin (KLH) using the bifunctional cross-linking reagent succinimidyl 4-(N-maleimidomethyl)cyclohexane-1-carboxylate (SMCC). Conjugation was performed with equal amounts of peptide to protein by weight (3:3 mg). A phospho-antigen sequence of Ac-C2887AKGGGS\*HPL2905amide (where S\* denotes phosphoserine) was synthesized using Fmoc chemistry and purified to 98.0% purity (as assessed by peak area integration of HPLC spectrogram and supported by LC-MS spectra). The phospho-antigen peptide was conjugated to the N-terminal cysteine residue to bovine serum albumin (BSA) using SMCC. Conjugation was performed with equal amounts of peptide to protein by weight (2:2 mg). A dephospho-peptide-antigen was also manufactured. Peptide Ac-C2887AKGGGSHPL2905amide was synthesized using Fmoc chemistry and purified to 94.65% purity (as assessed by peak area integration of HPLC spectrogram and supported by LC-MS spectra). The dephospho-antigen peptide was conjugated to the N-terminal cysteine residue to BSA using SMCC. Conjugation was performed with equal amounts of peptide to protein by weight (2:2 mg). In all cases, the peptide-protein conjugates were dialyzed into phosphatebuffered saline (PBS; pH 7.2) and lyophilized in 0.25-mg (immunogen) and 0.17-mg (antigen) units (weight represents theoretical protein weight) and stored dry at -20°C until used. The immunization protocol was initiated within 10 days of peptide conjugation.

The immunization work was performed in Germany, and all animal procedures were conducted in full compliance with the applicable German and European animal welfare legislation, specifically adhering to the German Animal Welfare Act (Tierschutzgesetz, TierSchG) and Directive 2010/63/EU of the European Parliament on the protection of animals used for scientific purposes. A single adult New Zealand white rabbit was immunized with 150 mg of immunogen peptide-KLH conjugate (quantity refers to theoretical KLH content) in Adjuvant P (Gerbu). Booster immunizations of 150 mg of immunogen peptide-KLH conjugate (quantity refers to theoretical KLH content) in Adjuvant S (Gerbu) were given on days 14, 28, 42, and 56, and a test bleed was conducted on day 35. A final bleed was performed on day 63, at which time the animal was euthanized.

Blood was allowed to clot at room temperature, and serum was collected by centrifugation and stored frozen at -20°C.

The recognition of phospho-antigen and the corresponding dephospho-antigen, in each case using antigen conjugated to BSA, was performed by enzyme-linked immunosorbent assay (ELISA). Microtiter plates (96 wells) were coated with antigen of 0.1 mg per well in 100 ml of 0.1 M NaHCO<sub>3</sub> (pH 8) overnight at 2° to 8°C. The wells were washed four times with 200 ml of wash buffer (1% NaCl/0.05% Tween 20), incubated for 5 min each time with shaking. Nonspecific protein binding sites were blocked in each well by incubation with 2% dried milk protein in 0.1 M NaHCO<sub>3</sub> (pH 8) and 0.05% Tween 20 for 30 min at room temperature. Wells were washed again, as before, and incubated with a 1:5 serial dilution of antiserum/ antibody in a final volume of 80 ml of PBS (pH 7.2) and 0.05% Tween 20. Incubations with primary antibody were performed overnight at 2° to 8°C. Wells were washed as before and incubated with alkaline phosphatase conjugated anti-rabbit immunoglobulin G (IgG) antibody (1:10,000) in PBS (pH 7.2) plus 0.05% Tween 20 for 2 hours at room temperature. Wells were washed as above and substrate (3.2 mM p-nitrophenyl phosphate) incubated for 2 hours in 1 M diethanolamine (pH 9.8). ELISA signals were recorded at 405 nm.

An automated Western blot was performed using the WES system (Protein Simple, CA, USA). A 12- to 230-kDa separation system was used for 10-fold serial dilution of phospho-antigen (pSer<sup>2902</sup>) in BSA in sample buffer from 10 mg/ml (10 to 0.01 mg/ml), along with the same 10-fold serial dilution of dephospho-antigen (Ser<sup>2902</sup>) in BSA (10 to 0.01 mg/ml). Detection was performed with a primary antibody dilution of 1:50 (purified IgG from final bleed, 8.08 mg/ml) and anti-rabbit IgG-peroxidase with chemiluminescence detection.

Total rabbit IgG was purified from the final bleed serum (day 63) using protein A affinity chromatography. IgG protein was eluted in 0.1 M citrate-phosphate buffer (pH 2.3) and immediately neutralized with tris. Protein was dialyzed against sodium acetate buffer with 0.02% sodium azide as antibacterial preservative. Purified IgG antibody protein (initial protein concentration of 10.1 mg/ml) was mixed with a sugar/organic polymer stabilizer formulation (20% by volume), reducing the protein concentration to 8.08 mg/ml. The antibody aliquots were frozen at  $-80^{\circ}$ C and freeze-dried. For long term storage, antibodies were desiccated at 4°C.

## SDS-polyacrylamide gel electrophoresis and Western blot

Experiments were performed as previously described with minor modifications (58, 108). Briefly, TA (tibialis anterior) muscles were thawed and homogenized using zirconium oxide beads (1.4 mm, Bertin Corp.) in radioimmunoprecipitation assay buffer. N-ethylmaleimide was added to 5 mM, and the samples were incubated on ice for 30 min. Total protein (60  $\mu$ g) was mixed with SDS sample buffer and denatured by heating at  $50^{\circ}$ C for 1 hour. Membranes were blocked for 30 min with EveryBlot blocking buffer (Bio-Rad) except for immunoblotting p-Ser $^{2902}$ , in which case we used Protein-Free T20 (PBS) blocking buffer (Pierce). Total protein and bands of interest were quantified by densitometry. Bands of interest were normalized to the total lane protein and expressed as a percentage of the average control (WT or FL) value on the same blot. All antibodies used are in table S2.

#### Statistical analysis

Appropriate statistical analyses were applied as specified in the figure legends using Prism10 (GraphPad). Sample size for each experiment

was determined from the SD of preliminary data. Values of P < 0.05(95% confidence) were considered statistically significant except for the proteomic studies where false discovery rate (FDR) was used to assess significance, and q < 0.05 was used (unless otherwise indicated). Values are presented as means  $\pm$  SD except for the force frequency, Ca<sup>2+</sup> frequency, and response curves (for caffeine, heat, and VA) where the data are shown as means  $\pm$  SEM to improve visualization. All statistical tests were two-sided. Differences between the two groups were analyzed for significance using Student's t tests and normality tests. If the data failed the normality tests, then we performed a Mann-Whitney rank sum test. Differences between means of multiple groups were analyzed by one- or two-way analysis of variance (ANOVA), and those with multiple individual myofibers per subject were analyzed by nested (hierarchical) ANOVA with Tukey post hoc tests. For Ca<sup>2+</sup> sparks, multiple FDB fibers from each mouse were analyzed, but we averaged all fibers (>4/mouse) per mouse of each genotype. Immunoprecipitations were first analyzed for specificity by comparing proteins in IgG controls with those in RYR1 immunoprecipitates. For discovery proteomics, data were analyzed with Holm-Šidák's multiple comparisons tests and/or calculation of the FDR. These values are plotted and compared as % control and analyzed by Student's t tests and normality tests. All measurements were taken from distinct samples. Outliers in the Ca<sup>2+</sup> data were identified by the Rout method (109) with Q set at 1% and removed to eliminate unhealthy fibers.

## **Supplementary Materials**

The PDF file includes:

Figs. S1 to S6 Tables S1 and S2

Other Supplementary Material for this manuscript includes the following: MDAR Reproducibility Checklist

#### **REFERENCES AND NOTES**

- D. C. Sheridan, H. Takekura, C. Franzini-Armstrong, K. G. Beam, P. D. Allen, C. F. Perez, Bidirectional signaling between calcium channels of skeletal muscle requires multiple direct and indirect interactions. *Proc. Natl. Acad. Sci. U.S.A.* 103, 19760–19765 (2006).
- R.T. Dirksen, Bi-directional coupling between dihydropyridine receptors and ryanodine receptors. Front. Biosci. 7, d659–d670 (2002).
- N. Ivarsson, C. M. Mattsson, A. J. Cheng, J. D. Bruton, B. Ekblom, J. T. Lanner, H. Westerblad, SR Ca<sup>2+</sup> leak in skeletal muscle fibers acts as an intracellular signal to increase fatigue resistance. *J. Gen. Physiol.* 151, 567–577 (2019).
- E. O. Hernández-Ochoa, S. J. P. Pratt, R. M. Lovering, M. F. Schneider, Critical role of intracellular RyR1 calcium release channels in skeletal muscle function and disease. Front. Physiol. 6, 420 (2015).
- A. Meizoso-Huesca, L. Pearce, C. J. Barclay, B. S. Launikonis, Ca<sup>2+</sup> leak through ryanodine receptor 1 regulates thermogenesis in resting skeletal muscle. *Proc. Natl. Acad. Sci. U.S.A.* 119, e2119203119 (2022).
- D. G. Stephenson, Modeling the mechanism of Ca<sup>2+</sup> release in skeletal muscle by DHPRs easing inhibition at RyR I1-sites. *J. Gen. Physiol.* 156, e202213113 (2024).
- C. J. Barclay, B. S. Launikonis, A mathematical model to quantify RYR Ca2+ leak and associated heat produciton in resting human skeletal muscle fibers. J. Gen. Physiol. 154, e202112994 (2022).
- T. R. Cully, R. H. Choi, A. R. Bjorksten, D. G. Stephenson, R. M. Murphy, B. S. Launikonis, Junctional membrane Ca2+ dynamics in human muscle fibers are altered by malignant hyperthermia causative mutation. *Proc. Natl. Acad. Sci. U.S.A.* 115, 8215–8220 (2018).
- B. S. Launikonis, E. Rios, Store-operated Ca<sup>2+</sup> entry during intracellular Ca<sup>2+</sup> release in mammalian skeletal muscle. *J. Physiol.* 583, 81–97 (2007).
- A. D. Lyfenko, R. T. Dirksen, Differential dependence of store-operated and excitationcoupled Ga<sup>2+</sup> entry in skeletal muscle on STIM1 and Orai1. J. Physiol. 586, 4815–4824 (2008).
- A. M. Bellinger, S. Reiken, C. Carlson, M. Mongillo, X. Liu, L. Rothman, S. Matecki, A. Lacampagne, A. R. Marks, Hypernitrosylated ryanodine receptor calcium release channels are leaky in dystrophic muscle. *Nat. Med.* 15, 325–330 (2009).

- A. Agrawal, G. Suryakumar, R. Rathor, Role of defective Ca<sup>2+</sup> signaling in skeletal muscle weakness: Pharmacological implications. J. Cell Commun. Signal. 12, 645–659 (2018).
- 13. L. Figueroa, N. Kraeva, C. Manno, S. Toro, E. Ríos, S. Riazi, Abnormal calcium signalling and the caffeine-halothane contracture test. *Br. J. Anaesth.* **122**, 32–41 (2019).
- M. G. Chelu, S. A. Goonasekera, W. J. Durham, W. Tang, J. D. Lueck, J. Riehl, I. N. Pessah, P. Zhang, M. B. Bhattacharjee, R. T. Dirksen, S. L. Hamilton, Heat- and anesthesia-induced malignant hyperthermia in an RyR1 knock-in mouse. FASEB J. 20, 329–330 (2006).
- H. J. Wang, C. S. Lee, R. S. Z. Yee, L. Groom, I. Friedman, L. Babcock, D. K. Georgiou, J. Hong, A. D. Hanna, J. Recio, J. M. Choi, T. Chang, N. H. Agha, J. Romero, P. Sarkar, N. Voermans, M. W. Gaber, S. Y. Jung, M. L. Baker, R. G. Pautler, R. T. Dirksen, S. Riazi, S. L. Hamilton, Adaptive thermogenesis enhances the life-threatening response to heat in mice with an Ryr1 mutation. *Nat. Commun.* 11, 5099 (2020).
- J.T. Lanner, D. K. Georgiou, A. Dagnino-Acosta, A. Ainbinder, Q. Cheng, A. D. Joshi, Z. Chen, V. Yarotskyy, J. M. Oakes, C. S. Lee, T. O. Monroe, A. Santillan, K. Dong, L. Goodyear, I. I. Ismailov, G. G. Rodney, R. T. Dirksen, S. L. Hamilton, AICAR prevents heat-induced sudden death in RyR1 mutant mice independent of AMPK activation. *Nat. Med.* 18, 244–251 (2012).
- E. R. Tammineni, N. Kraeva, L. Figueroa, C. Manno, C. A. Ibarra, A. Klip, S. Riazi, E. Rios, Intracellular calcium leak lowers glucose storage in human muscle, promoting hyperglycemia and diabetes. *eLife* 9, e53999 (2020).
- G. Santulli, R. Nakashima, Q. Yuan, A. R. Marks, Intracellular calcium release channels: An update. J. Physiol. 595, 3041–3051 (2017).
- E. V. de Lima Silva, K. C. Donis, F. R. C. Machado, L. Simão Medeiros, C. A. M. Aschoff, C. F. M. de Souza, F. O. Poswar, J. A. M. Saute, Oral dantrolene reduces myalgia and hyperckemia in a child with RYR1-related exertional myalgia/rhabdomyolysis. *J. Neuromuscul. Dis.* 10, 1145–1149 (2023).
- N. Dlamini, N. C. Voermans, S. Lillis, K. Stewart, E. J. Kamsteeg, G. Drost, R. Quinlivan, M. Snoeck, F. Norwood, A. Radunovic, V. Straub, M. Roberts, A. F. J. E. Vrancken, W. L. van der Pol, R. I. F. M. de Coo, A. Y. Manzur, S. Yau, S. Abbs, A. King, M. Lammens, P. M. Hopkins, S. Mohammed, S. Treves, F. Muntoni, E. Wraige, M. R. Davis, B. van Engelen, H. Jungbluth, Mutations in RYR1 are a common cause of exertional myalgia and rhabdomyolysis. *Neuromuscul. Disord.* 23, 540–548 (2013).
- N. Kruijt, L. V. den Bersselaar, M. Snoeck, K. Kramers, S. Riazi, C. Bongers, S. Treves, H. Jungbluth, N. Voermans, RYR1-related rhabdomyolysis: A spectrum of hypermetabolic states due to ryanodine receptor dysfunction. *Curr. Pharm. Des.* 28, 2–14 (2022).
- L. R. van den Bersselaar, N. Kruijt, G. J. Scheffer, L. van Eijk, I. Malagon, S. Buckens,
  J. A. E. Custers, L. Helder, A. Greco, L. A. B. Joosten, B. G. M. van Engelen, N. van Alfen,
  S. Riazi, S. Treves, H. Jungbluth, M. M. J. Snoeck, N. C. Voermans, The neuromuscular and
  multisystem features of RYR1-related malignant hyperthermia and rhabdomyolysis: A
  study protocol. *Medicine* 100, e26999 (2021).
- N. Kraeva, A. Sapa, J. J. Dowling, S. Riazi, Malignant hyperthermia susceptibility in patients with exertional rhabdomyolysis: A retrospective cohort study and updated systematic review. Can. J. Anaesth. 64, 736–743 (2017).
- N. Place, N. Ivarsson, T. Venckunas, D. Neyroud, M. Brazaitis, A. J. Cheng, J. Ochala, S. Kamandulis, S. Girard, G. Volungevičius, H. Paužas, A. Mekideche, B. Kayser, V. Martinez-Redondo, J. L. Ruas, J. Bruton, A. Truffert, J. T. Lanner, A. Skurvydas, H. Westerblad, Ryanodine receptor fragmentation and sarcoplasmic reticulum Ca<sup>2+</sup> leak after one session of high-intensity interval exercise. *Proc. Natl. Acad. Sci. U.S.A.* 112, 15492–15497 (2015).
- N. Zanou, H. Dridi, S. Reiken, T. Imamura de Lima, C. Donnelly, U. de Marchi, M. Ferrini, J. Vidal, L. Sittenfeld, J. N. Feige, P. M. Garcia-Roves, I. C. Lopez-Mejia, A. R. Marks, J. Auwerx, B. Kayser, N. Place, Acute RyR1 Ca<sup>2+</sup> leak enhances NADH-linked mitochondrial respiratory capacity. *Nat. Commun.* 12, 7219 (2021).
- D. C. Andersson, M. J. Betzenhauser, S. Reiken, A. C. Meli, A. Umanskaya, W. Xie, T. Shiomi, R. Zalk, A. Lacampagne, A. R. Marks, Ryanodine receptor oxidation causes intracellular calcium leak and muscle weakness in aging. *Cell Metab.* 14, 196–207 (2011).
- R. A. Casuso, J. R. Huertas, The emerging role of skeletal muscle mitochondrial dynamics in exercise and ageing. Ageing Res. Rev. 58, 101025 (2020).
- Y. S. Prakash, I. Seckin, L. W. Hunter, G. C. Sieck, Mechanisms underlying greater sensitivity
  of neonatal cardiac muscle to volatile anesthetics. *Anesthesiology* 96, 893–906 (2002).
- C. F. Louis, K. Zualkernan, T. Roghair, J. R. Mickelson, The effects of volatile anesthetics on calcium regulation by malignant hyperthermia-susceptible sarcoplasmic reticulum. *Anesthesiology* 77, 114–125 (1992).
- W. J. Durham, P. Aracena-Parks, C. Long, A. E. Rossi, S. A. Goonasekera, S. Boncompagni, D. L. Galvan, C. P. Gilman, M. R. Baker, N. Shirokova, F. Protasi, R. Dirksen, S. L. Hamilton, RyR1 S-nitrosylation underlies environmental heat stroke and sudden death in Y522S RyR1 knockin mice. Cell 133, 53–65 (2008).
- S. Z. Ali, A. Taguchi, H. Rosenberg, Malignant hyperthermia. Best Pract. Res. Clin. Anaesthesiol. 17, 519–533 (2003).
- M. Serano, L. Pietrangelo, C. Paolini, F. A. Guarnier, F. Protasi, Oxygen consumption and basal metabolic rate as markers of susceptibility to malignant hyperthermia and heat stroke. Cells 11, 2468 (2022).

- T. Yamazawa, T. Kobayashi, N. Kurebayashi, M. Konishi, S. Noguchi, T. Inoue, Y. U. Inoue,
  I. Nishino, S. Mori, H. Iinuma, N. Manaka, H. Kagechika, A. Uryash, J. Adams, J. R. Lopez,
  X. Liu, C. Diggle, P. D. Allen, S. Kakizawa, K. Ikeda, B. Lin, Y. Ikemi, K. Nunomura,
  S. Nakagawa, T. Sakurai, T. Murayama, A novel RyR1-selective inhibitor prevents and
  rescues sudden death in mouse models of malignant hyperthermia and heat stroke. Nat.
  Commun. 12, 4293 (2021).
- O. Laitano, K. O. Murray, L. R. Leon, Overlapping mechanisms of exertional heat stroke and malignant hyperthermia: Evidence vs. conjecture. Sports Med. 50, 1581–1592 (2020).
- K. Oyama, V. Zeeb, T. Yamazawa, N. Kurebayashi, F. Kobirumaki-Shimozawa, T. Murayama, H. Oyamada, S. Noguchi, T. Inoue, Y. U. Inoue, I. Nishino, Y. Harada, N. Fukuda, S. Ishiwata, M. Suzuki, Heat-hypersensitive mutants of ryanodine receptor type 1 revealed by microscopic heating. *Proc. Natl. Acad. Sci. U.S.A.* 119, e2201286119 (2022).
- E. M. Gallant, J. Hart, K. Eager, S. Curtis, A. F. Dulhunty, Caffeine sensitivity of native RyR channels from normal and malignant hyperthermic pigs: Effects of a DHPR II-III loop peptide. Am. J. Physiol. Cell Physiol. 286, C821–C830 (2004).
- M. Wehner, H. Rueffert, F. Koenig, J. Neuhaus, D. Olthoff, Increased sensitivity to 4-chloro-m-cresol and caffeine in primary myotubes from malignant hyperthermia susceptible individuals carrying the ryanodine receptor 1 Thr2206Met (C6617T) mutation. Clin. Genet. 62, 135–146 (2002).
- M. Haseeb, P. D. Thompson, The effect of statins on RyR and RyR-associated disease. J. Appl. Physiol. 131, 661–671 (2021).
- M. Knoblauch, A. Dagnino-Acosta, S. L. Hamilton, Mice with RyR1 mutation (Y524S) undergo hypermetabolic response to simvastatin. Skelet. Muscle 3, 22 (2013).
- R. R. Johi, R. Mills, P. J. Halsall, P. M. Hopkins, Anaesthetic management of coronary artery bypass grafting in a patient with central core disease and susceptibility to malignant hyperthermia on statin therapy. Br. J. Anaesth. 91, 744–747 (2003).
- K. D. Marciante, J. P. Durda, S. R. Heckbert, T. Lumley, K. Rice, B. McKnight, R. A. Totah, B. Tamraz, D. L. Kroetz, H. Fukushima, R. Kaspera, J. C. Bis, N. L. Glazer, G. Li, T. R. Austin, K. D. Taylor, J. I. Rotter, C. E. Jaquish, P. Y. Kwok, R. P. Tracy, B. M. Psaty, Cerivastatin, genetic variants, and the risk of rhabdomyolysis. *Pharmacogenet. Genomics* 21, 280–288 (2011).
- G. D. Vladutiu, P. J. Isackson, K. Kaufman, J. B. Harley, B. Cobb, L. Christopher-Stine, R. L. Wortmann, Genetic risk for malignant hyperthermia in non-anesthesia-induced myopathies. *Mol. Genet. Metab.* 104, 167–173 (2011).
- J. J. Todd, T. A. Lawal, I. C. Chrismer, A. Kokkinis, C. Grunseich, M. S. Jain, M. R. Waite, V. Biancavilla, S. Pocock, K. Brooks, C. J. Mendoza, G. Norato, K. Cheung, W. Riekhof, P. Varma, C. Colina-Prisco, M. Emile-Backer, K. G. Meilleur, A. R. Marks, Y. Webb, E. E. Marcantonio, A. R. Foley, C. G. Bönnemann, P. Mohassel, Rycal S48168 (ARM210) for RYR1-related myopathies: A phase one, open-label, dose-escalation trial. EClinicalMedicine 68, 102433 (2024).
- J. J. Todd, T. A. Lawal, J. W. Witherspoon, I. C. Chrismer, M. S. Razaqyar, M. Punjabi, J. S. Elliott, F. Tounkara, A. Kuo, M. O. Shelton, C. Allen, M. M. Cosgrove, M. Linton, D. Michael, M. S. Jain, M. Waite, B. Drinkard, P. G. Wakim, J. J. Dowling, C. G. Bönnemann, M. Emile-Backer, K. G. Meilleur, Randomized controlled trial of N-acetylcysteine therapy for RYR1-related myopathies. Neurology 94, e1434–e1444 (2020).
- K. A. Iyer, Y. Hu, T. Klose, T. Murayama, M. Samsó, Molecular mechanism of the severe MH/ CCD mutation Y522S in skeletal ryanodine receptor (RyR1) by cryo-EM. *Proc. Natl. Acad. Sci. U.S.A.* 119, e2122140119 (2022).
- G. Robin, B. Allard, Dihydropyridine receptors actively control gating of ryanodine receptors in resting mouse skeletal muscle fibres. J. Physiol. 590, 6027–6036 (2012).
- M. Gaburjakova, J. Gaburjakova, S. Reiken, F. Huang, S. O. Marx, N. Rosemblit, A. R. Marks, FKBP12 binding modulates ryanodine receptor channel gating. *J. Biol. Chem.* 276, 16931–16935 (2001).
- A. Meizoso-Huesca, C. R. Lamboley, J. R. Krycer, M. P. Hodson, J. E. Hudson,
   S. Launikonis, Muscle-specific ryanodine receptor 1 properties underlie limb-girdle muscular dystrophy 2B/R2 progression. *Nat. Commun.* 16, 3056 (2025).
- W. Shou, B. Aghdasi, D. L. Armstrong, Q. Guo, S. Bao, M. J. Charng, L. M. Mathews, M. D. Schneider, S. L. Hamilton, M. M. Matzuk, Cardiac defects and altered ryanodine receptor function in mice lacking FKBP12. *Nature* 391, 489–492 (1998).
- S. Reiken, A. Lacampagne, H. Zhou, A. Kherani, S. E. Lehnart, C. Ward, F. Huang, M. Gaburjakova, J. Gaburjakova, N. Rosemblit, M. S. Warren, K. L. He, G. H. Yi, J. Wang, D. Burkhoff, G. Vassort, A. R. Marks, PKA phosphorylation activates the calcium release channel (ryanodine receptor) in skeletal muscle: Defective regulation in heart failure. *J. Cell Biol.* 160, 919–928 (2003).
- C. S. Lee, D. K. Georgiou, A. Dagnino-Acosta, J. Xu, I. I. Ismailov, M. Knoblauch, T. O. Monroe, R. R. Ji, A. D. Hanna, A. D. Joshi, C. Long, J. Oakes, T. Tran, B. T. Corona, S. Lorca, C. P. Ingalls, V. A. Narkar, J. T. Lanner, J. H. Bayle, W. J. Durham, S. L. Hamilton, Ligands for FKBP12 increase Ca<sup>2+</sup> influx and protein synthesis to improve skeletal muscle function. *J. Biol. Chem.* 289, 25556–25570 (2014).
- H. Dridi, M. Yehya, R. Barsotti, S. Reiken, C. Angebault, B. Jung, S. Jaber, A. R. Marks, A. Lacampagne, S. Matecki, Mitochondrial oxidative stress induces leaky ryanodine receptor during mechanical ventilation. Free Radic. Biol. Med. 146, 383–391 (2020).

- M. M. Steinz, N. Beard, E. Shorter, J. T. Lanner, Stable oxidative posttranslational modifications alter the gating properties of RyR1. J. Gen. Physiol. 156, e202313515 (2024).
- D. Sato, B. Ghayoumi, A. Fasoli, C. Y. Ko, D. M. Bers, Positive feedback between RyR phosphorylation and Ca<sup>2+</sup> leak promotes heterogeneous Ca<sup>2+</sup> release. *Biophys. J.* 124, 717–721 (2025).
- D. C. Andersson, M. J. Betzenhauser, S. Reiken, A. Umanskaya, T. Shiomi, A. R. Marks, Stress-induced increase in skeletal muscle force requires protein kinase A phosphorylation of the ryanodine receptor. *J. Physiol.* **590**, 6381–6387 (2012).
- L. M. Blayney, J. L. Jones, J. Griffiths, F. A. Lai, A mechanism of ryanodine receptor modulation by FKBP12/12.6, protein kinase A, and K201. *Cardiovasc. Res.* 85, 68–78 (2010)
- H. M. Campbell, A. P. Quick, I. Abu-Taha, D. Y. Chiang, C. F. Kramm, T. A. Word,
   S. Brandenburg, M. Hulsurkar, K. M. Alsina, H. B. Liu, B. Martin, D. Uhlenkamp,
   O. M. Moore, S. K. Lahiri, E. Corradini, M. Kamler, A. J. R. Heck, S. E. Lehnart, D. Dobrev,
   X. H. T. Wehrens, Loss of SPEG inhibitory phosphorylation of ryanodine receptor type-2 promotes atrial fibrillation. *Circulation* 142, 1159–1172 (2020).
- C. S. Lee, S. Y. Jung, R. S. Z. Yee, N. H. Agha, J. Hong, T. Chang, L. W. Babcock,
   J. D. Fleischman, B. Clayton, A. D. Hanna, C. S. Ward, D. Lanza, A. E. Hurley, P. Zhang,
   X. H. T. Wehrens, W. R. Lagor, G. G. Rodney, S. L. Hamilton, Speg interactions that regulate the stability of excitation-contraction coupling protein complexes in triads and dyads.
   Commun. Biol. 6, 942 (2023).
- V. Huntoon, J. J. Widrick, C. Sanchez, S. M. Rosen, C. Kutchukian, S. Cao, C. R. Pierson, X. Liu, M. A. Perrella, A. H. Beggs, V. Jacquemond, P. B. Agrawal, SPEG-deficient skeletal muscles exhibit abnormal triad and defective calcium handling. *Hum. Mol. Genet.* 27, 1608–1617 (2018).
- Q. Li, J. Lin, S. Luo, K. Schmitz-Abe, R. Agrawal, M. Meng, B. Moghadaszadeh, A. H. Beggs, X. Liu, M. A. Perrella, P. B. Agrawal, Integrated multi-omics approach reveals the role of striated muscle preferentially expressed protein kinase in skeletal muscle including its relationship with myospryn complex. *J. Cachexia. Sarcopenia Muscle* 15, 1003–1015 (2024).
- C. Quan, M. Li, Q. du, Q. Chen, H. Wang, D. Campbell, L. Fang, B. Xue, C. MacKintosh, X. Gao, K. Ouyang, H. Y. Wang, S. Chen, SPEG controls calcium reuptake into the sarcoplasmic reticulum through regulating SERCA2a by its second kinase-domain. *Circ. Res.* 124, 712–726 (2019).
- A. P. Quick, Q. Wang, L. E. Philippen, G. Barreto-Torres, D. Y. Chiang, D. Beavers, G. Wang, M. Khalid, J. O. Reynolds, H. M. Campbell, J. Showell, M. D. McCauley, A. Scholten, X. H. T. Wehrens, SPEG (striated muscle preferentially expressed protein kinase) is essential for cardiac function by regulating junctional membrane complex activity. *Circ. Res.* 120, 110–119 (2017).
- J. R. Lopez, V. Kaura, C. P. Diggle, P. M. Hopkins, P. D. Allen, Malignant hyperthermia, environmental heat stress, and intracellular calcium dysregulation in a mouse model expressing the p.G2435R variant of RYR1. Br. J. Anaesth. 121, 953–961 (2018).
- G. C. Barrientos, W. Feng, K. Truong, K. I. Matthaei, T. Yang, P. D. Allen, J. R. Lopez, I. N. Pessah, Gene dose influences cellular and calcium channel dysregulation in heterozygous and homozygous T4826I-RYR1 malignant hyperthermia-susceptible muscle. J. Biol. Chem. 287, 2863–2876 (2012).
- W. Feng, G. C. Barrientos, G. Cherednichenko, T. Yang, I. T. Padilla, K. Truong, P. D. Allen, J. R. Lopez, I. N. Pessah, Functional and biochemical properties of ryanodine receptor type 1 channels from heterozygous R163C malignant hyperthermia-susceptible mice. *Mol. Pharmacol.* 79, 420–431 (2011).
- K. A. Quane, K. E. Keating, J. M. S. Healy, B. M. Manning, R. Krivosic-Horber, I. Krivosic, N. Monnier, J. Lunardi, T. V. McCarthy, Mutation screening of the RYR1 gene in malignant hyperthermia: Detection of a novel Tyr to Ser mutation in a pedigree with associated central cores. *Genomics* 23, 236–239 (1994).
- A. des Georges, O. B. Clarke, R. Zalk, Q. Yuan, K. J. Condon, R. A. Grassucci,
   W. A. Hendrickson, A. R. Marks, J. Frank, Structural basis for gating and activation of RyR1. Cell 167, 145–157.e17 (2016).
- X. C. Bai, Z. Yan, J. Wu, Z. Li, N. Yan, The central domain of RyR1 is the transducer for long-range allosteric gating of channel opening. *Cell Res.* 26, 995–1006 (2016).
- S. Cholak, J. W. Saville, X. Zhu, A. M. Berezuk, K. S. Tuttle, O. Haji-Ghassemi, F. J. Alvarado, F. van Petegem, S. Subramaniam, Allosteric modulation of ryanodine receptor RyR1 by nucleotide derivatives. *Structure* 31, 790–800.e4 (2023).
- A. R. Nayak, W. Rangubpit, A. H. Will, Y. Hu, P. Castro-Hartmann, J. J. Lobo, K. Dryden, G. D. Lamb, P. Sompornpisut, M. Samsó, Interplay between Mg<sup>2+</sup> and Ca<sup>2+</sup> at multiple sites of the ryanodine receptor. *Nat. Commun.* 15, 4115 (2024).
- C. Manno, L. Figueroa, L. Royer, S. Pouvreau, C. S. Lee, P. Volpe, A. Nori, J. Zhou, G. Meissner, S. L. Hamilton, E. Ríos, Altered Ca<sup>2+</sup> concentration, permeability and buffering in the myofibre Ca<sup>2+</sup> store of a mouse model of malignant hyperthermia. *J. Physiol.* 591, 4439–4457 (2013).
- R. E. Loy, M. Orynbayev, L. Xu, Z. Andronache, S. Apostol, E. Zvaritch, D. H. MacLennan,
   G. Meissner, W. Melzer, R. T. Dirksen, Muscle weakness in Ryr1I4895T/WT knock-in mice as

- a result of reduced ryanodine receptor Ca<sup>2+</sup> ion permeation and release from the sarcoplasmic reticulum. *J. Gen. Physiol.* **137**, 43–57 (2011).
- A. Michelucci, S. Boncompagni, L. Pietrangelo, T. Takano, F. Protasi, R. T. Dirksen, Pre-assembled Ca<sup>2+</sup> entry units and constitutively active Ca<sup>2+</sup> entry in skeletal muscle of calsequestrin-1 knockout mice. *J. Gen. Physiol.* 152, e202012617 (2020).
- C. R. Lamboley, L. Pearce, C. Seng, A. Meizoso-Huesca, D. P. Singh, B. P. Frankish, V. Kaura, H. P. Lo, C. Ferguson, P. D. Allen, P. M. Hopkins, R. G. Parton, R. M. Murphy, C. van der Poel, C. J. Barclay, B. S. Launikonis, Ryanodine receptor leak triggers fiber Ca<sup>2+</sup> redistribution to preserve force and elevate basal metabolism in skeletal muscle. *Sci. Adv.* 7, eabi7166 (2021).
- S. K. Lahiri, J. Lu, Y. Aguilar-Sanchez, H. Li, L. M. Moreira, M. M. Hulsurkar, A. Mendoza, M. R. Turkieltaub Paredes, J. A. Navarro-Garcia, E. Munivez, B. Horist, O. M. Moore, G. Weninger, S. Brandenburg, C. Lenz, S. E. Lehnart, R. Sayeed, G. Krasopoulos, V. Srivastava, L. Zhang, J. M. Karch, S. Reilly, X. H. T. Wehrens, Targeting calpain-2mediated junctophilin-2 cleavage delays heart failure progression following myocardial infarction. J. Mol. Cell. Cardiol. 194, 85–95 (2024).
- J. Wang, G. Ciampa, D. Zheng, Q. Shi, B. Chen, E. D. Abel, T. Peng, D. D. Hall, L. S. Song, Calpain-2 specifically cleaves Junctophilin-2 at the same site as Calpain-1 but with less efficacy. *Biochem. J.* 478, 3539–3553 (2021).
- S. K. Lahiri, A. P. Quick, B. Samson-Couterie, M. Hulsurkar, I. Elzenaar, R. J. van Oort, X. H. T. Wehrens, Nuclear localization of a novel calpain-2 mediated junctophilin-2 C-terminal cleavage peptide promotes cardiomyocyte remodeling. *Basic Res. Cardiol.* 115, 49 (2020).
- H. L. Huang, S. C. Li, J. F. Wu, A complex of novel protease inhibitor, ovostatin homolog, with its cognate proteases in immature mice uterine luminal fluid. Sci. Rep. 9, 4973 (2019).
- Y. Noda, H. Miyoshi, S. Benucci, A. Gonzalez, O. Bandschapp, T. Girard, S. Treves, F. Zorzato, Functional characterization of RYR1 variants identified in malignant hyperthermia susceptible individuals. *Neuromuscul. Disord.* 33, 951–963 (2023).
- W. Klingler, S. Heiderich, T. Girard, E. Gravino, J. J. A. Heffron, S. Johannsen, K. Jurkat-Rott, H. Rüffert, F. Schuster, M. Snoeck, V. Sorrentino, V. Tegazzin, F. Lehmann-Horn, Functional and genetic characterization of clinical malignant hyperthermia crises: A multi-centre study. Orphanet J. Rare Dis. 9, 8 (2014).
- R. Weisshorn, F. Wappler, M. Fiege, M. U. Gerbershagen, K. Kolodzie, P. Alberts, E. P. Horn, J. Schulte am Esch, Ryanodine contracture threshold times for diagnosis of malignant hyperthermia susceptibility: An experimental approach from a single laboratory. J. Clin. Anesth. 16. 353–357 (2004).
- S. Riazi, L. R. van den Bersselaar, G. Islander, L. Heytens, M. M. J. Snoeck, A. Bjorksten, R. Gillies, G. Dranitsaris, A. Hellblom, S. Treves, G. Kunst, N. C. Voermans, H. Jungbluth, Pre-operative exercise and pyrexia as modifying factors in malignant hyperthermia (MH). Neuromuscul. Disord. 32, 628–634 (2022).
- H. Campbell, Y. Aguilar-Sanchez, A. P. Quick, D. Dobrev, X. H. T. Wehrens, SPEG: A key regulator of cardiac calcium homeostasis. *Cardiovasc. Res.* 117, 2175–2185 (2021).
- P. B. Agrawal, C. R. Pierson, M. Joshi, X. Liu, G. Ravenscroft, B. Moghadaszadeh, T. Talabere, M. Viola, L. C. Swanson, G. Haliloğlu, B. Talim, K. S. Yau, R. J. Allcock, N. G. Laing, M. A. Perrella, A. H. Beggs, SPEG interacts with myotubularin, and its deficiency causes centronuclear myopathy with dilated cardiomyopathy. *Am. J. Hum. Genet.* 95, 218–226 (2014).
- X. Liu, T. Ramjiganesh, Y.-H. Chen, S. W. Chung, S. R. Hall, S. L. Schissel, R. F. Padera Jr., R. Liao, K. G. Ackerman, J. Kajstura, A. Leri, P. Anversa, S.-F. Yet, M. D. Layne, M. A. Perrella, Disruption of striated preferentially expressed gene locus leads to dilated cardiomyopathy in mice. *Circulation* 119, 261–268 (2009).
- L. Pearce, A. Meizoso-Huesca, C. Seng, C. R. Lamboley, D. P. Singh, B. S. Launikonis, Ryanodine receptor activity and store-operated Ca<sup>2+</sup> entry: Critical regulators of Ca<sup>2+</sup> content and function in skeletal muscle. *J. Physiol.* 601, 4183–4202 (2023).
- M. Canato, P. Capitanio, L. Cancellara, L. Leanza, A. Raffaello, D. V. Reane, L. Marcucci, A. Michelucci, F. Protasi, C. Reggiani, Excessive accumulation of Ca<sup>2+</sup> in mitochondria of Y522S-RYR1 knock-in mice: A link between leak from the sarcoplasmic reticulum and altered redox state. Front. Physiol. 10, 1142 (2019).
- V. R. Chirasani, D. A. Pasek, G. Meissner, Structural and functional interactions between the Ca<sup>2+</sup>-, ATP-, and caffeine-binding sites of skeletal muscle ryanodine receptor (RyR1). *J. Biol. Chem.* 297, 101040 (2021).
- R. M. Murphy, T. L. Dutka, D. Horvath, J. R. Bell, L. M. Delbridge, G. D. Lamb, Ca<sup>2+</sup> dependent proteolysis of junctophilin-1 and junctophilin-2 in skeletal and cardiac muscle. *J. Physiol.* 591, 719–729 (2013).
- M. DiFranco, I. Kramerova, J. L. Vergara, M. J. Spencer, Attenuated Ca<sup>2+</sup> release in a mouse model of limb girdle muscular dystrophy 2A. Skelet. Muscle 6, 11 (2016).
- K. Kanzaki, D. Watanabe, M. Kuratani, T. Yamada, S. Matsunaga, M. Wada, Role of calpain in eccentric contraction-induced proteolysis of Ca<sup>2+</sup>-regulatory proteins and force depression in rat fast-twitch skeletal muscle. *J. Appl. Physiol.* 122, 396–405 (2017).
- V. Shoshan-Barmatz, S. Weil, H. Meyer, M. Varsanyi, L. M. Heilmeyer, Endogenous, Ca<sup>2+</sup>-dependent cysteine-protease cleaves specifically the ryanodine receptor/Ca<sup>2+</sup> release channel in skeletal muscle. *J. Membr. Biol.* 142, 281–288 (1994).
- G. G. Rodney, B. Y. Williams, G. M. Strasburg, K. Beckingham, S. L. Hamilton, Regulation of RYR1 activity by Ca<sup>2+</sup> and calmodulin. *Biochemistry* 39, 7807–7812 (2000).

- R.T. Rebbeck, B. Svensson, J. Zhang, M. Samsó, D. D. Thomas, D. M. Bers, R. L. Cornea, Kinetics and mapping of Ca-driven calmodulin conformations on skeletal and cardiac muscle ryanodine receptors. *Nat. Commun.* 15, 5120 (2024).
- J. Zhang, L. M. Treinen, S. J. Mast, M. R. M. Carthy, B. Svensson, D. D. Thomas, R. L. Cornea, Kinetics insight into the roles of the N- and C-lobes of calmodulin in RyR1 channel regulation. J. Biol. Chem. 301, 108258 (2025).
- B. R. Fruen, D. J. Black, R. A. Bloomquist, J. M. Bardy, J. D. Johnson, C. F. Louis, E. M. Balog, Regulation of the RYR1 and RYR2 Ca<sup>2+</sup> release channel isoforms by Ca<sup>2+</sup>-insensitive mutants of calmodulin. *Biochemistry* 42, 2740–2747 (2003).
- E. M. Balog, L. E. Norton, R. A. Bloomquist, R. L. Cornea, D. J. Black, C. F. Louis, D. D. Thomas, B. R. Fruen, Calmodulin oxidation and methionine to glutamine substitutions reveal methionine residues critical for functional interaction with ryanodine receptor-1. *J. Biol. Chem.* 278, 15615–15621 (2003).
- A. Tripathy, L. Xu, G. Mann, G. Meissner, Calmodulin activation and inhibition of skeletal muscle Ca<sup>2+</sup> release channel (ryanodine receptor). *Biophys. J.* 69, 106–119 (1995).
- K. Godbout, M. Dugas, S. R. Reiken, S. Ramezani, A. Falle, J. Rousseau, A. E. Wronska, G. Lamothe, G. Canet, Y. Lu, E. Planel, A. R. Marks, J. P. Tremblay, Universal prime editing therapeutic strategy for RyR1-related myopathies: A protective mutation rescues leaky RyR1 channel. *Int. J. Mol. Sci.* 26, 2835 (2025).
- C. Liang, S. Malik, M. He, L. Groom, S. K. Ture, T. N. O'Connor, C. N. Morrell, R. T. Dirksen, Compound heterozygous RYR1-RM mouse model reveals disease pathomechanisms and muscle adaptations to promote postnatal survival. FASEB J. 38, e70120 (2024).
- W. C. Skarnes, B. Rosen, A. P. West, M. Koutsourakis, W. Bushell, V. Iyer, A. O. Mujica, M. Thomas, J. Harrow, T. Cox, D. Jackson, J. Severin, P. Biggs, J. Fu, M. Nefedov, P. J. de Jong, A. F. Stewart, A. Bradley, A conditional knockout resource for the genome-wide study of mouse gene function. *Nature* 474, 337–342 (2011).
- J. C. Brüning, M. D. Michael, J. N. Winnay, T. Hayashi, D. Hörsch, D. Accili, L. J. Goodyear,
   C. R. Kahn, A muscle-specific insulin receptor knockout exhibits features of the metabolic syndrome of NIDDM without altering glucose tolerance. *Mol. Cell* 2, 559–569 (1998).
- D. G. Lanza, J. Mao, I. Lorenzo, L. Liao, J. R. Seavitt, M. C. Ljungberg, E. M. Simpson,
   F. J. DeMayo, J. D. Heaney, An oocyte-specific Cas9-expressing mouse for germline CRISPR/Cas9-mediated genome editing. *Genesis* 62, e23589 (2024).
- R. I. Close, Dynamic properties of mammalian skeletal muscles. *Physiol. Rev.* 52, 129–197 (1972)
- A. D. Hanna, C. S. Lee, L. Babcock, H. Wang, J. Recio, S. L. Hamilton, Pathological mechanisms of vacuolar aggregate myopathy arising from a Casq1 mutation. FASEB J. 35, e21349 (2021).
- 106. C. R. H. Lamboley, S. A. K. Guena, F. Touré, C. Hébert, L. Yaddaden, S. Nadeau, P. Bouchard, L. W.-L. Pierre, J. Lainé, E. C. Rousseau, J. Frenette, F. Protasi, R. T. Dirksen, P. C. Pape, New method for determining total calcium content in tissue applied to skeletal muscle with and without calsequestrin. J. Gen. Physiol. 145, 127–153 (2015).
- D. M. Bers, C. W. Patton, R. Nuccitelli, A practical guide to the preparation of Ca<sup>2+</sup> buffers. Methods Cell Biol. 40, 3–29 (1994).
- 108. A. D. Hanna, T. Chang, K. S. Ho, R. S. Z. Yee, W. C. Walker, N. Agha, C. W. Hsu, S. Y. Jung, M. E. Dickinson, M. A. H. Samee, C. S. Ward, C. S. Lee, G. G. Rodney, S. L. Hamilton, Mechanisms underlying dilated cardiomyopathy associated with FKBP12 deficiency. *J. Gen. Physiol.* 157, e202413583 (2025).
- H. J. Motulsky, R. E. Brown, Detecting outliers when fitting data with nonlinear regression A new method based on robust nonlinear regression and the false discovery rate. BMC Bioinformatics 7, 123 (2006).

Acknowledgments: We thank the directors and staff at the Genetically Engineered Rat and Mouse Core, the Mouse Metabolism and Phenotyping Core, the Optical Imaging and Vital Microscopy Cores at BCM, and the Genetically Engineered Rodent Model (GERM) Core at BCM. The Mouse Metabolism and Phenotyping Core is supported by RO1DK114356, UM1HG006348, and \$100D032380. The GERM Core is funded, in part, by the National Institutes of Health Cancer Center Grant (P30 CA125123). Funding: This work was supported by the National Institutes of Health [National Institute of Arthritis and Musculoskeletal and Skin Diseases (NIAMS)] grants 1R21AR082613-01 (C.S.L.), R01AR061370 (G.G.R.), and R01AR082209 (S.L.H.) and by the Muscular Dystrophy Association, 960053 (G.G.R.). Author contributions: Conceptualization: S.L.H. and G.G.R. Methodology: R.S.Z.Y., C.S.L., T.C., S.Y.J., O.Y., C.C., J.C., F.Y.P., G.G.R., and S.L.H. Investigation: R.S.Z.Y., C.S.L., T.C., S.Y.J., O.Y., C.C., J.C., F.Y.P., G.G.R., and S.L.H. Visualization: S.L.H. Supervision: G.G.R. and S.L.H. Writing—original draft: R.S.Z.Y. and S.L.H. Writing—review and editing: All authors. Competing interests: J.C. is a shareholder, director, and employee of Badrilla Ltd., a life science reagents company that manufactures antibody products for research use only. The other authors declare that they have no competing interests. Data and materials availability: The MS data for proteome profiling have been deposited in the ProteomeXchange Consortium with the dataset identifier PXD060589 (https://proteomecentral.proteomexchange.org/cgi/ GetDataset?ID=PXD060589) at the MASSIVE repository [https://massive.ucsd.edu/ProteoSAFe/ dataset.isp?task=8aff256bffa34d188e9e67a2382b26a6 (MSV 000097079)]. The complete dataset has been deposited at Dryad (10.5061/dryad.r2280gbpr). All other data needed to evaluate the conclusions in the paper are present in the paper or the Supplementary Materials.

The code written in IDL to analyze  $Ca^{2+}$  spark data has been deposited in Zenodo (https://doi.org/10.5281/zenodo.17023652). The YS and S2902D mice used in this study are available from S.L.H. under a material transfer agreement with BCM. The p-Ser<sup>2902</sup> antibody is available upon request from S.L.H.

Submitted 8 March 2025 Accepted 15 September 2025 Published 7 October 2025 10.1126/scisignal.adx3087